



**Politecnico
di Torino**

Politecnico di Torino

Master of Science Course in Materials Engineering

A.Y. 2020/2021

Graduation session October 2021

Development of ternary biopolymer blends: mechanical and rheological characterization

Tutors:

Prof. Alberto Frache

Prof. Rossella Arrigo

Candidate:

Maria Falomo

Table of contents

Riassunto della tesi.....	IV
List of figures	XX
List of tables	XXII
1. Introduction	1
2. Ternary blends.....	3
2.1 Thermodynamics of polymeric blends.....	4
2.2 Flory-Huggins theory	4
2.3 Effect of interfacial forces on blend morphologies.....	5
2.4 Background of PLA-based ternary blends	7
3. Materials and methods	15
3.1 Materials.....	15
3.2 Blend preparation	15
3.3 Characterization techniques	17
3.3.1 Differential Scanning Calorimetry (DSC).....	17
3.3.2 Rheological measurements.....	18
3.3.3 Scanning Electron Microscopy (SEM)	19
3.3.4 Mechanical measurements	19
4. Results and discussion.....	23
4.1 Selection of the most ductile blend formulation	23
4.2 PLA/PBS/PHBH blends	26
4.2.1 Differential Scanning Calorimetry (DSC).....	27
4.2.2 Rheological measurements.....	31
4.2.3 Scanning Electron Microscopy (SEM)	35
4.2.4 Mechanical measurements	38
4.3 50PLA/40PBS/10PHBH blend	40
5. Conclusions	41
6. References	43

Riassunto della tesi

I. Obiettivo

L'obiettivo di questo lavoro è realizzare un blend ternario allo scopo di incrementare l'allungamento a rottura di PLA e PHBH utilizzando un polimero duttile come PBAT, PBSA e PBS, pur mantenendo elevati valori di modulo e massimo stress caratteristici di PLA e PHBH.

II. Risultati

II.I Selezione della formulazione più duttile

È stata eseguita una caratterizzazione preliminare delle proprietà meccaniche dei blend 50PLA/30PBAT/20PHBH, 50PLA/30PBSA/20PHBH e 50PLA/30PBS/20PHBH, al fine di scegliere la formulazione più adatta a soddisfare il requisito iniziale.

Osservando le proprietà meccaniche riportate in Tabella II.I e la curva sforzo-deformazione in Figura II.I, è possibile notare come il blend 50PLA/30PBAT/20PHBH abbia un comportamento fragile. Esso presenta un allungamento a rottura del 14%, di molto inferiore rispetto all'allungamento del PBAT puro che risulta del 623%, ciò suggerisce che il PBAT non abbia un effetto di miglioramento della duttilità del blend. Inoltre, durante il processo di estrusione, il blend 50PLA/30PBAT/20PHBH ha mostrato una forte instabilità del flusso anche in seguito alla regolazione dei parametri di processo. Quindi, a causa delle scarse proprietà meccaniche e della scarsa lavorabilità, tale formulazione non è stata ulteriormente esaminata.

Tabella II.I Proprietà meccaniche del blend 50PLA/30PBAT/20PHBH.

Modulo (MPa)	5188 ± 1036
Deformazione al massimo stress(%)	3 ± 1
Massimo stress (MPa)	40 ± 3
Allungamento a rottura (%)	14 ± 2
Sforzo a rottura (MPa)	4 ± 1

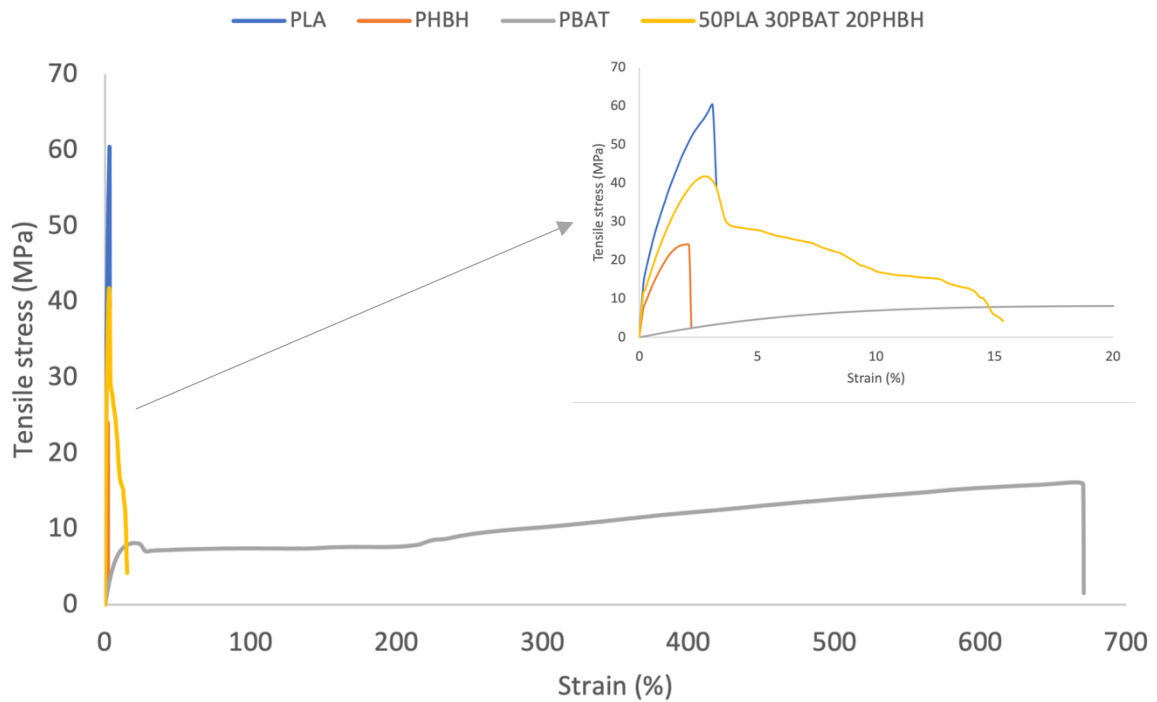


Figura 11.I Curva sforzo-deformazione del blend 50PLA/30PBAT/20PHBH rispetto a PLA, PBAT e PHBH.

Come si può osservare dalle proprietà meccaniche riportate in Tabella II.II e dalla curva sforzo-deformazione in Figura II.II, il blend 50PLA/30PBSA/20PHBH, ha un allungamento a rottura pari al 6%, che è inferiore rispetto al blend 50PLA/30PBAT/20PHBH. L'introduzione del PBSA non ha fornito quindi un miglioramento dell'allungamento a rottura del blend, di conseguenza, anche tale formulazione non è stata ulteriormente esaminata.

Tabella II.II Proprietà meccaniche del blend 50PLA/30PBSA/20PHBH.

Modulo (MPa)	2536 ± 164
Deformazione al massimo stress (%)	3 ± 1
Massimo stress (MPa)	45 ± 2
Allungamento a rottura (%)	6 ± 1
Sforzo a rottura (MPa)	21 ± 1

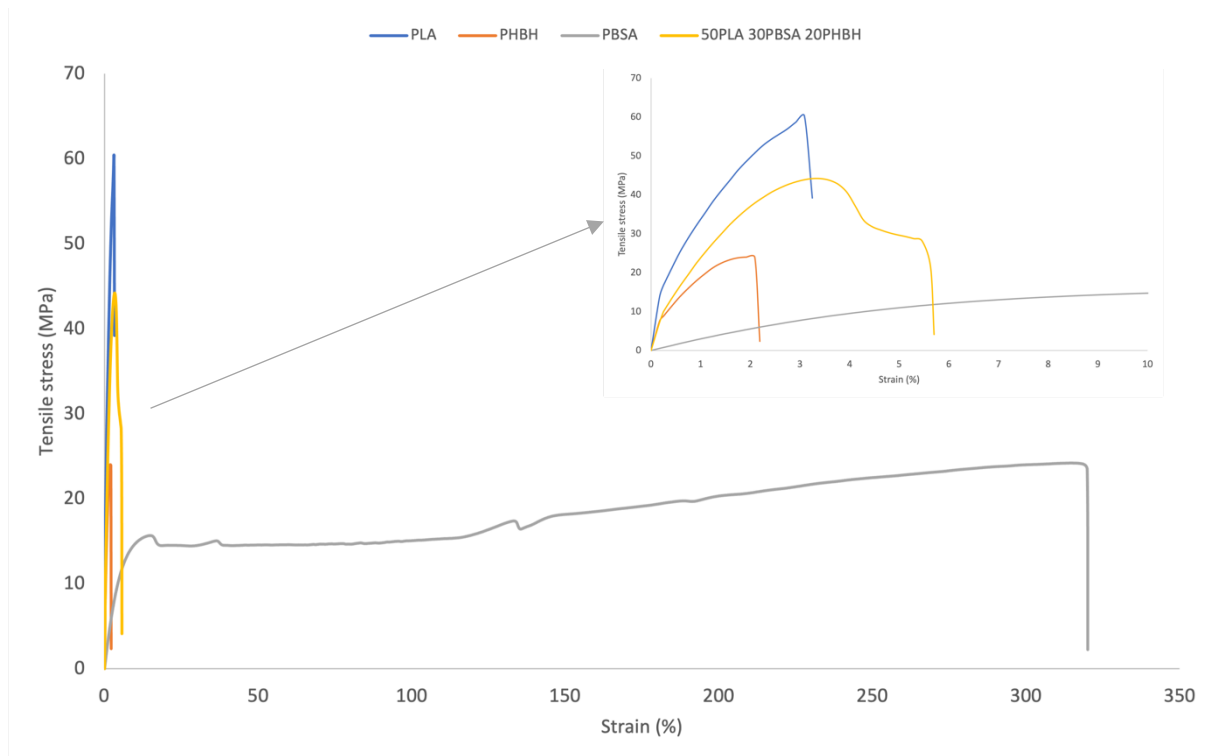


Figura II.II Curva sforzo-deformazione del blend 50PLA/30PBS/20PHBH rispetto a PLA, PBSA e PHBH.

Il blend 50PLA/30PBS/20PHBH ha mostrato invece un miglioramento consistente delle proprietà meccaniche, avendo un allungamento a rottura pari al 157%, come si può osservare in Tabella II.III e in Figura II.III. Dato tale miglioramento, il PBS è stato utilizzato per lo sviluppo delle altre formulazioni, la cui caratterizzazione è riportata nei paragrafi successivi.

Tabella II.III Proprietà meccaniche del blend 50PLA/30PBS/20PHBH.

Modulo (MPa)	1841 ± 452
Deformazione al massimo stress (%)	4 ± 1
Massimo stress (MPa)	43 ± 1
Allungamento a rottura (%)	157 ± 42
Sforzo a rottura (MPa)	24 ± 4

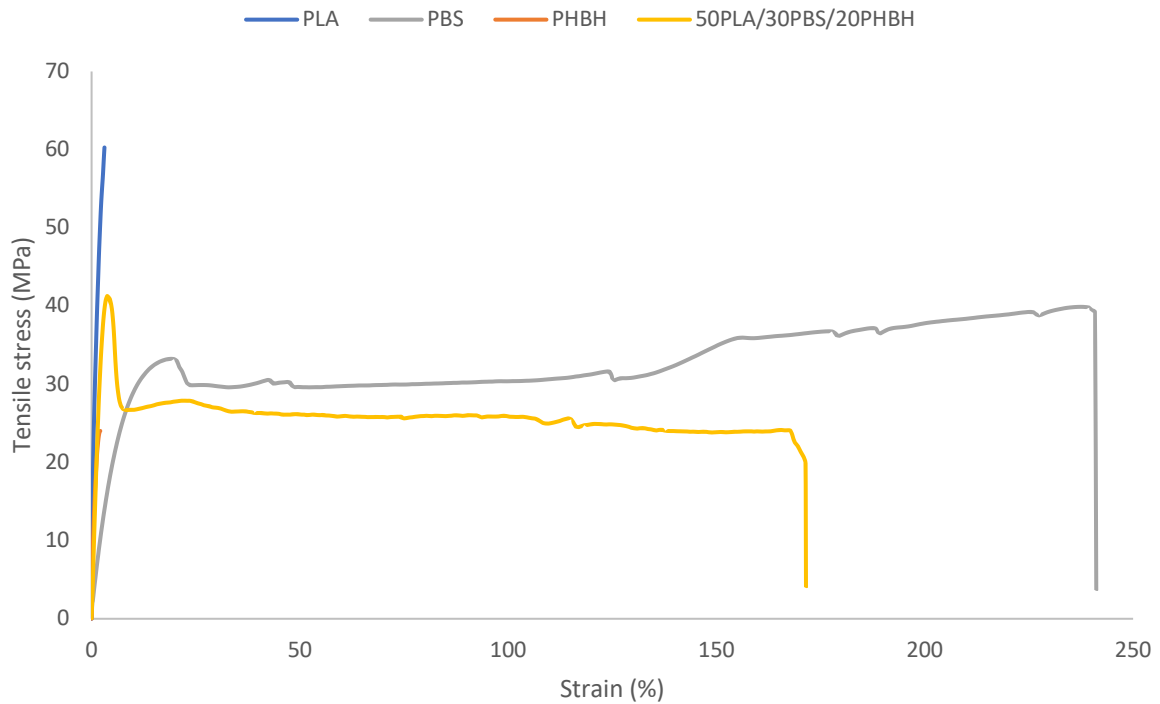


Figura 2.III Curva sforzo-deformazione del blend 50PLA/30PBS/20PHBH rispetto a PLA, PBS e PHBH.

II.II Blend PLA/PBS/PHBH

La formulazione 50PLA/30PBS/20PHBH si è rivelata la migliore nel soddisfare l'obiettivo prefissato, pertanto sono state valutate altre formulazioni con variazioni del contenuto di PLA e PHBH. Per comodità, di seguito verranno indicate solo con le loro composizioni, la quali sono riassunte nel diagramma ternario in Figura II.IV.

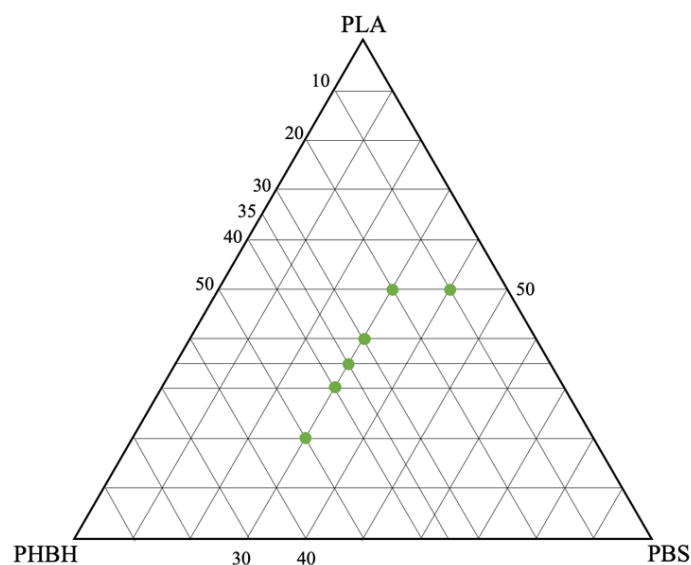


Figura II.IV Diagramma ternario della composizione dei blend PLA/PBS/PHBH.

II.II.I Calorimetria differenziale a scansione (DSC)

Le curve di raffreddamento dei blend PLA/PBS/PHBH e dei polimeri puri derivanti dall'analisi DSC sono riportate in Figura II.V. Dall'osservazione delle curve è possibile notare come all'aumentare del contenuto di PHBH nei blend, il picco di cristallizzazione del PBS si sposti a temperature inferiori fino a coincidere con il picco di cristallizzazione del PHBH. La cristallizzazione del PBS potrebbe essere quindi limitata dalla presenza del PHBH. D'altra parte, all'aumentare del contenuto di PLA, i picchi di cristallizzazione del PHBH si spostano a temperature inferiori rispetto al PHBH puro; PLA e PBS potrebbero quindi limitare la cristallizzazione del PHBH. La diminuzione della percentuale di cristallizzazione potrebbe essere causata dall'effetto di diluizione tra le fasi, che riduce il numero di catene macromolecolari che raggiungono i cristalli in crescita.

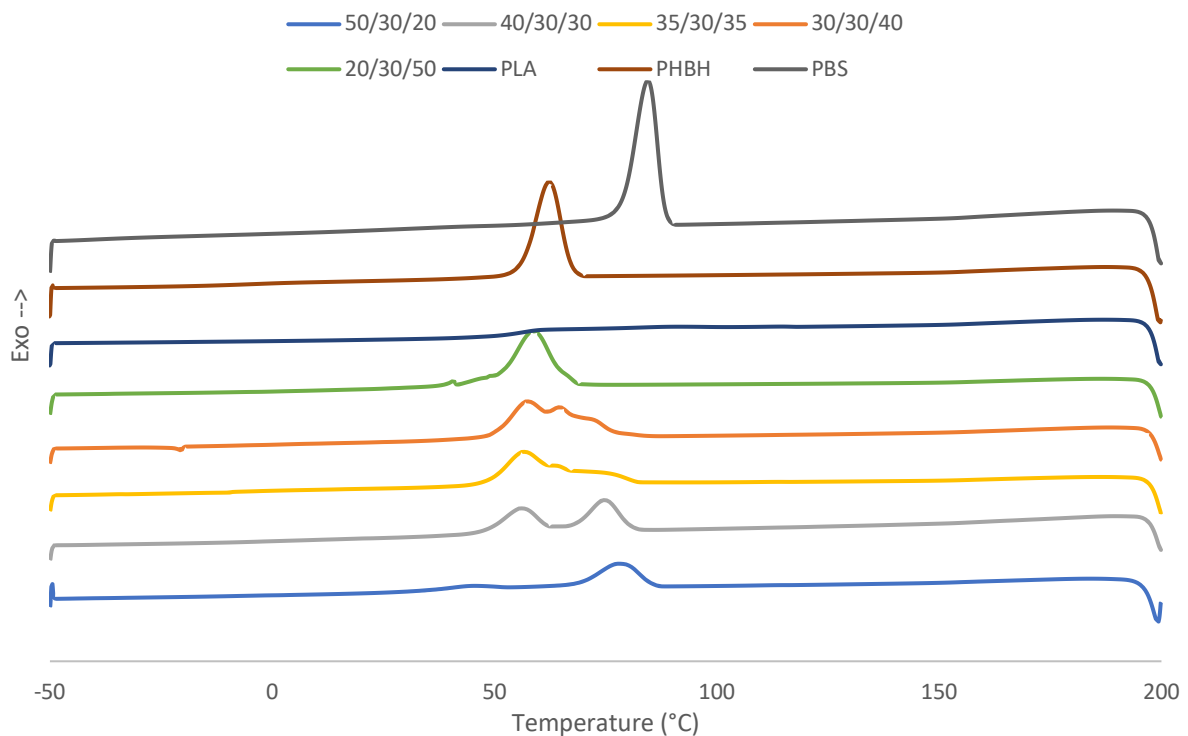


Figura II.V Curve DSC di raffreddamento dei blend PLA/PBS/PHBH e dei polimeri puri.

Le curve DSC del secondo riscaldamento dei blend PLA/PBS/PHBH e dei polimeri puri sono riportate in Figura II.VI. In tutti i blend è possibile individuare la temperatura di transizione vetrosa del PLA, la quale rimane costante a circa 58 °C, mentre non è possibile individuare quella di PHBH e PBS. I tre picchi endotermici presenti nelle curve relative ai blend sono attribuibili alla fusione delle fasi, le temperature di fusione di PLA, PHBH e PBS corrispondono a quelle dei polimeri puri e sono rispettivamente 168 °C, 148 °C e 113 °C. Il picco esotermico relativo alla cold crystallization del PLA nei blend si sposta a temperature leggermente inferiori rispetto al PLA puro. Considerando che il PHBH e il PBS hanno miscibilità limitata con il PLA, le loro fasi amorfe potrebbero attivare la mobilità delle catene di PLA e promuoverne la cold crystallization come conseguenza dell'allineamento dinamico delle catene nel materiale. Inoltre, la superficie di PHBH e PBS potrebbe comportarsi da centro di nucleazione favorendo la cristallizzazione del PLA.

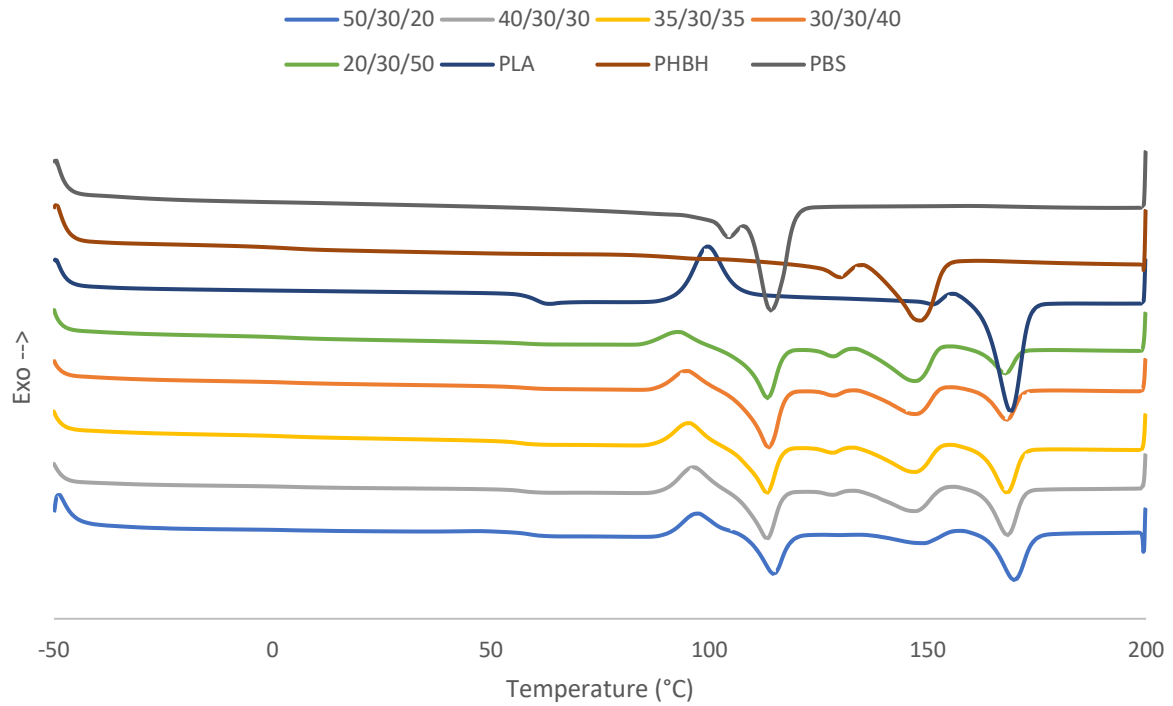


Figura II.VI Curve DSC del secondo riscaldamento dei blend PLA/PBS/PHBH e dei polimeri puri.

La Tabella II.IV riassume le principali proprietà termiche, misurate durante il secondo riscaldamento, di ciascuna fase presente nei blend.

Tabella II.IV Principali proprietà termiche dei blend PLA/PBS/PHBH.

Blend	Proprietà	PLA	PBS	PHBH
50/30/20	Tg (°C)	59	-	-
	Tm (°C)	170	115	149
	ΔH_m (J/g)	21	12	7
	Tcc (°C)	97	-	-
	ΔH_{cc} (J/g)	12	-	-
	χ (%)	9	11	5
40/30/30	Tg (°C)	57	-	-
	Tm (°C)	168	113	147
	ΔH_m (J/g)	18	17	16
	Tcc (°C)	96	-	-
	ΔH_{cc} (J/g)	12	-	-
	χ (%)	6	16	11
35/30/35	Tg (°C)	57	-	-
	Tm (°C)	168	113	147
	ΔH_m (J/g)	18	17	18
	Tcc (°C)	95	-	-
	ΔH_{cc} (J/g)	13	-	-
	χ (%)	6	16	12
30/30/40	Tg (°C)	57	-	-
	Tm (°C)	168	114	148
	ΔH_m (J/g)	12	24	17
	Tcc (°C)	95	-	-
	ΔH_{cc} (J/g)	9	-	-
	χ (%)	4	22	12
20/30/50	Tg (°C)	58	-	-
	Tm (°C)	168	113	148
	ΔH_m (J/g)	10	21	22
	Tcc (°C)	93	-	-
	ΔH_{cc} (J/g)	7	-	-
	χ (%)	4	19	15

II.II.II Prove reologiche

In Figura II.VII sono riportate le curve relative all'andamento della viscosità complessa in funzione della frequenza. Il PLA presenta il comportamento tipico dei materiali newtoniani, la curva relativa alla viscosità presenta infatti un plateau in tutto l'intervallo di frequenze analizzato. Al contrario, il PBS ha un comportamento notevolmente non-newtoniano, poiché la zona di shear-thinning è estesa a tutto l'intervallo di frequenze esaminato. Il PHBH ha invece, a basse frequenze, un comportamento di yield stress, con un rapido decremento di viscosità in corrispondenza di piccole variazioni di frequenza. Tale comportamento è tipico di polimeri contenenti filler minerali, ed è correlato alla limitazione del processo di rilassamento delle macromolecole, la quale è dovuta alla diminuzione della mobilità delle catene causata dall'instaurarsi di interazioni polimero-filler o filler-filler. La presenza di una carica minerale all'interno del PHBH è stata confermata dall'osservazione al SEM (Sezione II.II.III).

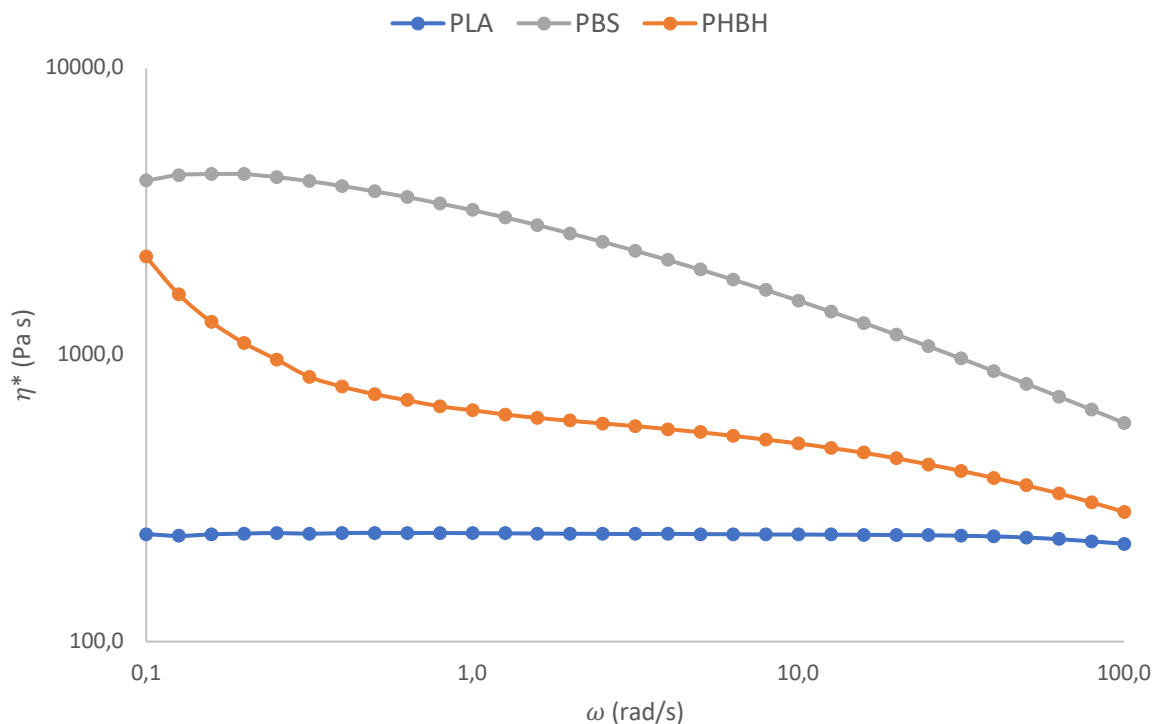


Figura II.VII Viscosità complessa in funzione della frequenza di PLA, PBS e PHBH puri.

In Figura II.VIII sono riportate le curve della viscosità complessa dei blend in funzione della frequenza. In generale la viscosità sembra essere maggiormente influenzata dal contenuto di PLA e PHBH, in quanto il contenuto di PBS non ha una forte influenza sul trend delle curve, soprattutto nei blend a maggiore contenuto di PHBH; tale comportamento potrebbe essere dovuto alla presenza di un filler minerale nel PHBH puro che influenza fortemente la viscosità dei blend.

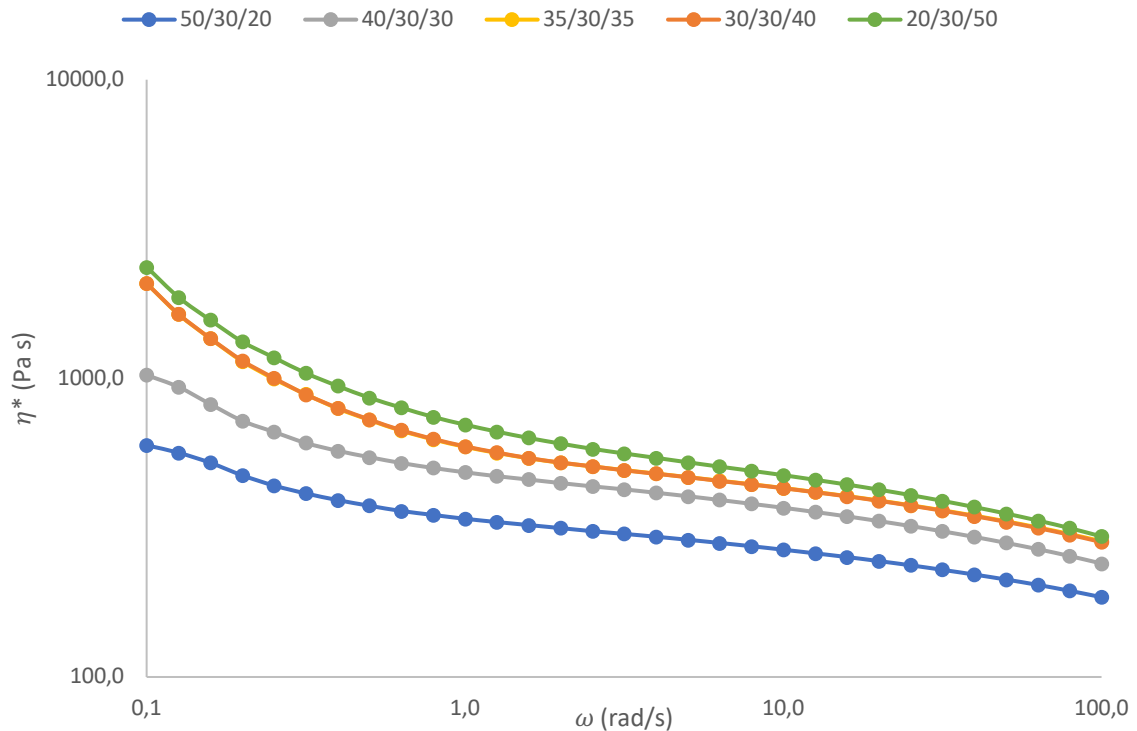


Figura II.VIII Viscosità complessa dei blend in funzione della frequenza.

Le curve relative all'andamento del modulo conservativo G' dei blend riportate in Figura II.IX non mostrano il tipico flesso presente nelle curve di blend immiscibili, ciò potrebbe suggerire la presenza di un certo grado di compatibilità tra i polimeri o il raggiungimento di una morfologia fine e omogenea. Ad alte frequenze i valori di G' sono intermedi rispetto a quelli dei polimeri puri, le dinamiche a corto raggio delle macromolecole non sono quindi influenzate dalla presenza di interfacce tra le fasi in questo intervallo di frequenze. Al contrario a basse e medie frequenze il modulo conservativo presenta valori più elevati rispetto ai polimeri puri; tale comportamento è attribuibile a un'amplificazione del comportamento elastico dei materiali derivante dalla morfologia trifasica dei blend. La presenza di interfacce tra le fasi e il verificarsi di fenomeni di rilassamento delle fasi disperse soggette a un flusso di taglio, comporta un aumento di G' rispetto ai polimeri puri. Inoltre, i blend contenenti una maggiore quantità di PHBH presentano valori di G' più elevati in tutto l'intervallo di frequenze investigato, tale comportamento potrebbe essere associato sia al maggior contenuto di carica minerale sia a una morfologia più fine.

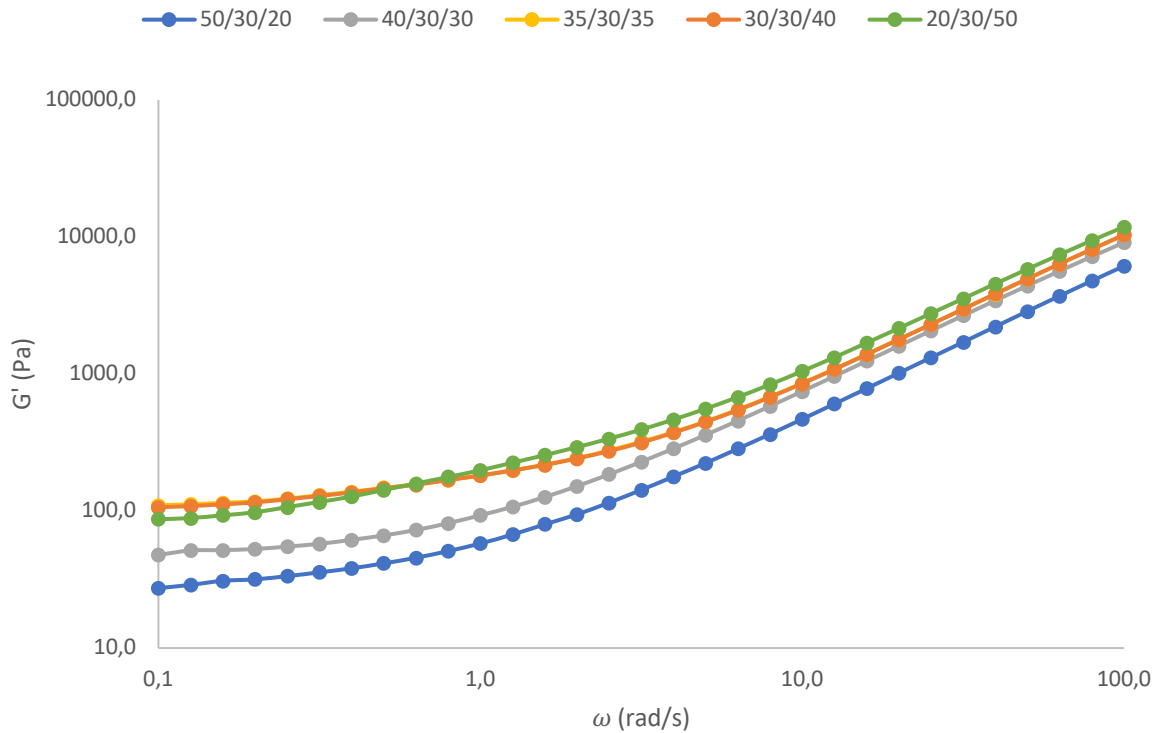


Figura II.IX Curve del modulo conservativo G' dei blend in funzione della frequenza.

II.II.III Microscopia elettronica a scansione (SEM)

La caratteristica più evidente emersa dall'osservazione delle immagini SEM dei campioni non trattati dei blend, è la presenza di lamelle, indice della presenza di un filler minerale nel PHBH puro. Per investigare ulteriormente il contenuto di filler nel PHBH, il campione non trattato del blend 20/30/50 è stato sottoposto a spettroscopia EDS e a termogravimetria (TGA). Lo spettro risultante dall'analisi EDS riportato in Figura II.X ha confermato la presenza di silicio e magnesio, i quali sono contenuti nel talco ($Mg_3Si_4O_{10}(OH)_2$), minerale utilizzato normalmente nei biopolimeri come agente nucleante. Dall'analisi TGA del PHBH puro, è emerso che non sono presenti residui a 340 °C, probabilmente a causa del ridotto contenuto di talco al suo interno. È stata quindi dimostrata la presenza di piccole quantità di talco nel PHBH e la sua distribuzione e dispersione ottimale sia nel PHBH puro che nei blend. Il comportamento di yield stress osservato durante le prove reologiche è quindi riconducibile al contenuto di filler che deve essere preso in considerazione nella caratterizzazione dei blend, in particolare quelli a matrice PHBH.

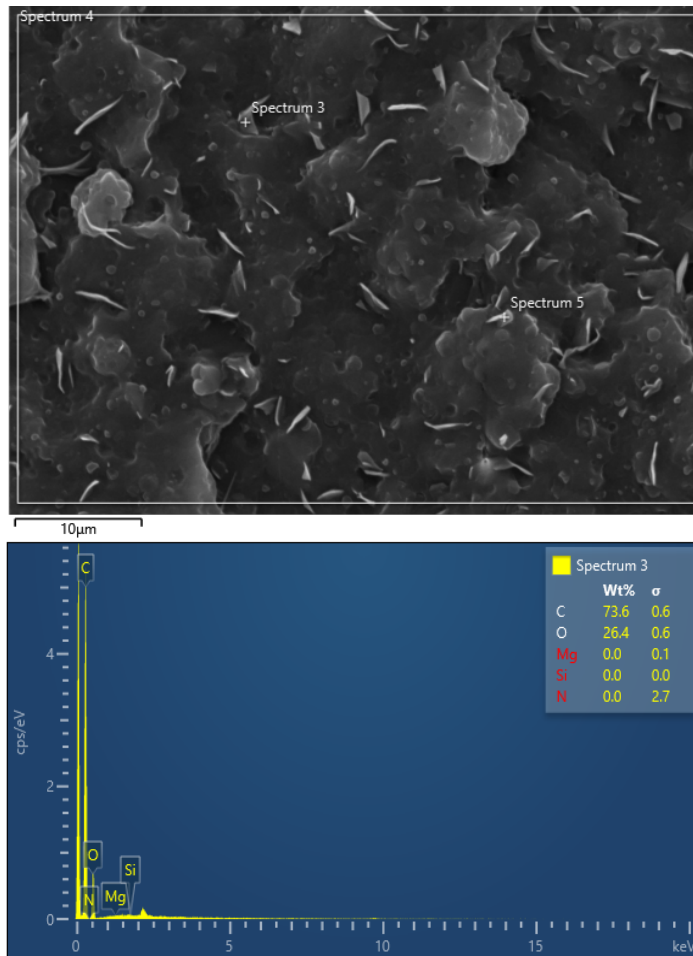


Figura II.X Spettro EDS di una lamella presente nel campione del blend 20/30/50.

Osservando le immagini SEM più significative riportate in Figura II.XI, è possibile notare come sia presente la morfologia droplet-like tipica dei blend immiscibili. La superficie delle fasi disperse non mostra bordi netti e definiti e appare piuttosto ruvida, si ipotizza quindi ci sia un certo grado di compatibilità e adesione interfacciale tra le fasi. Nei blend a matrice PLA (Figura II.XI a, b) le fasi disperse sembrano avere dimensioni maggiori rispetto ai blend a matrice PHBH (Figura II.XI d, e). Una morfologia più fine potrebbe significare una maggiore adesione tra le fasi e un migliore comportamento meccanico, tuttavia tale ipotesi sarà smentita dalle prove meccaniche.

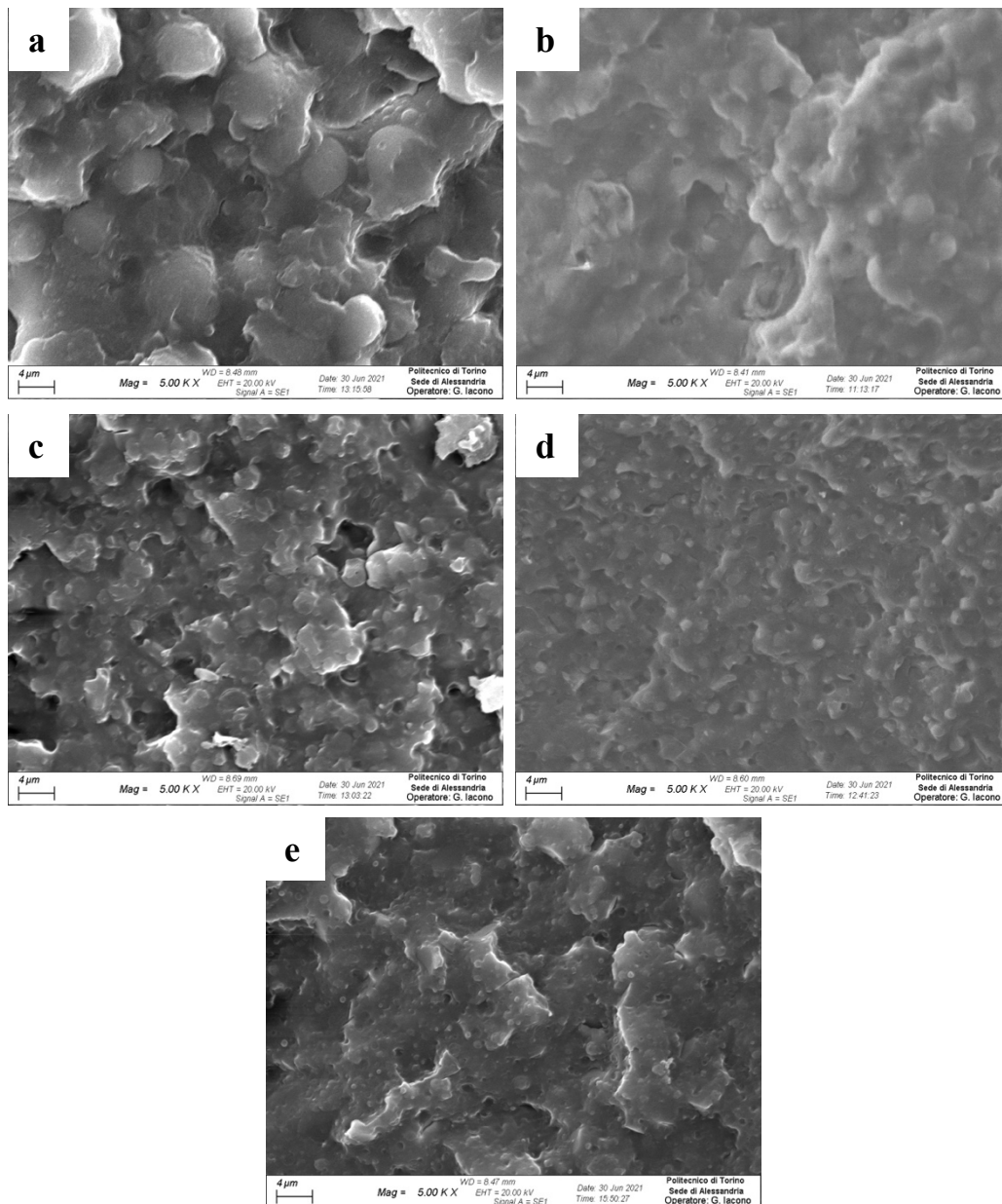


Figura II.XI Immagini SEM delle superfici di frattura dei blend trattate con acido acetico: a) 50/30/20, b) 40/30/30, c) 35/30/35, d) 30/30/40 and e) 20/30/50 a ingrandimento 5000x.

II.II.IV Prove meccaniche

I risultati delle prove meccaniche dei blend sono riportati in Figura II.XII e le principali proprietà meccaniche sono riassunte in Tabella II.V. Rispetto al PLA puro e il PHBH puro, che hanno un allungamento del 3% e del 2% rispettivamente, tutti i blend hanno mostrato una maggiore duttilità, con allungamenti dal 7% al 157%. Tutti i campioni hanno mostrato un comportamento a frattura duttile, al contrario di PLA e PHBH che mostravano frattura fragile. Il massimo stress delle miscele è risultato migliorato rispetto al PBS puro e al PHBH puro, ma leggermente ridotto rispetto al PLA puro.

Il modulo è risultato essere più alto rispetto al PBS puro e al PHBH puro, variando da 1670 MPa a 1871 MPa, ma inferiore quasi del 66% rispetto al PLA puro.

Come accennato in precedenza, l'allungamento a rottura è superiore rispetto al PLA puro e al PHBH puro in tutti i blend, anche se solo in quelli a matrice PLA il miglioramento è considerevole. I blend 50/30/20 e 40/30/30 hanno infatti un allungamento del 157% e del 46%

rispettivamente, mentre i blend 35/30/35, 30/30/40 e 20/30/50 soltanto dell'8%, 7%, e 12% rispettivamente. All'aumentare del contenuto di PHBH diminuisce la duttilità dei blend, sia per le proprietà meccaniche caratteristiche del PHBH puro, sia per la presenza di talco al suo interno.

La tenacità è stata calcolata per ciascun blend come area media sottesa alla curva sforzo-deformazione. I blend a maggiore contenuto di PLA hanno una tenacità di un ordine di grandezza superiore rispetto ai blend a maggiore contenuto di PHBH.

Confrontando i risultati derivanti dall'analisi DSC, è possibile notare come, all'aumentare del contenuto di PHBH, aumentino le percentuali di cristallinità di PHBH e PBS, mentre nei blend a maggiore contenuto di PLA, esse siano piuttosto contenute. A un maggiore grado di cristallinità è infatti associata una maggiore fragilità dei materiali, la quale è stata confermata dalle prove meccaniche. I valori più elevati del modulo conservativo G' , evidenziati dalle prove reologiche e attribuibili sia a una morfologia più fine che a un contenuto di talco più elevato, sono in accordo con il comportamento più elastico, e quindi più fragile, dei blend a matrice PHBH. La presenza di interfacce tra le fasi e una morfologia fine ed omogenea emerse valutando l'andamento di G' , sono state confermate dall'analisi SEM. Le immagini SEM hanno dimostrato la presenza di una buona adesione tra le fasi, caratteristica che contribuisce al raggiungimento di proprietà meccaniche elevate.

Dalle prove meccaniche è quindi possibile concludere che la combinazione di elevata rigidità e buona duttilità dei blend in esame, normalmente impossibile da ottenere con polimeri puri, apre applicazioni finora inaccessibili ai soli PLA, PBS e PHBH.

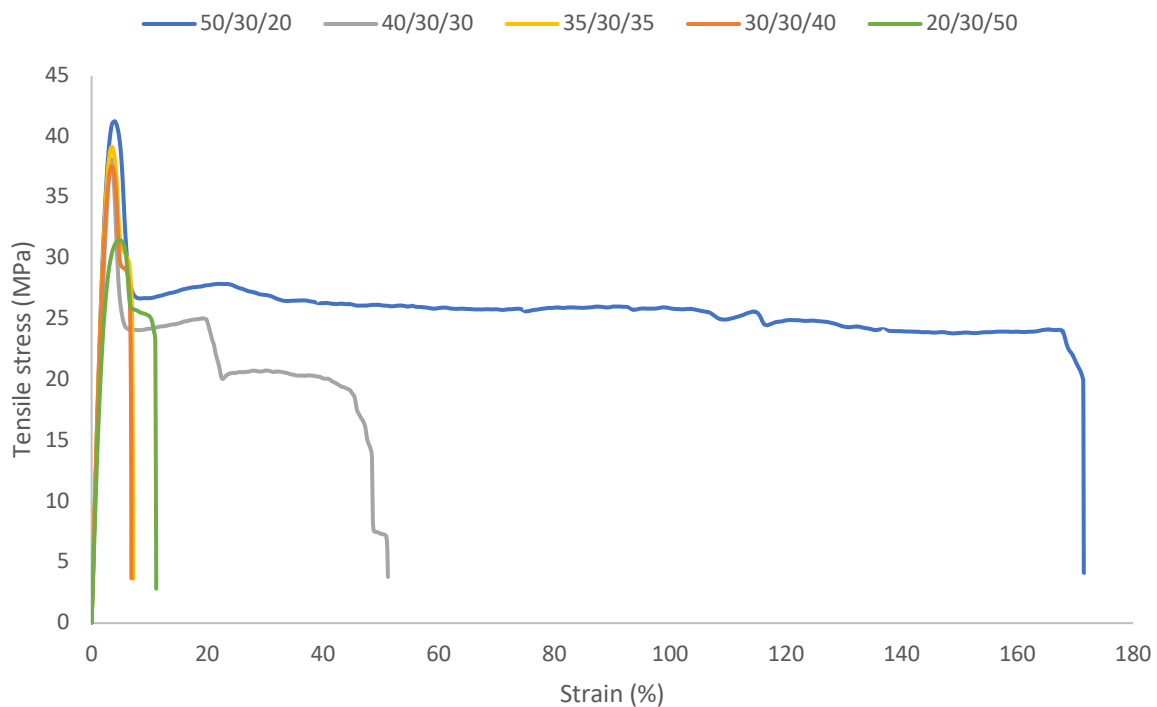


Figura II.XII Curve sforzo-deformazione dei blend PLA/PBS/PHBH.

Tabella II.V Principali proprietà meccaniche dei blend PLA/PBS/PHBH.

Proprietà	50/30/20	40/30/30	35/30/35	30/30/40	20/30/50
Modulo (MPa)	1841 ± 452	1763 ± 38	1744 ± 16	1670 ± 39	1341 ± 29
Deformazione al massimo stress (%)	4 ± 1	4 ± 1	3 ± 1	3 ± 1	5 ± 1
Massimo stress (MPa)	43 ± 1	42 ± 3	37 ± 3	37 ± 1	31 ± 1
Allungamento a rottura (%)	157 ± 42	46 ± 13	8 ± 1	7 ± 1	12 ± 1
Sforzo a rottura (MPa)	24 ± 4	11 ± 9	12 ± 5	21 ± 3	19 ± 5
Tenacità (J/m ³)	4124	1220	207	199	286

II.III Blend 50PLA/40PBS/10PHBH

Per migliorare ulteriormente l'allungamento a rottura dei blend PLA/PBS/PHBH è stata sviluppata la formulazione 50/40/10, le cui proprietà meccaniche sono riportate in Tabella II.VI. L'allungamento a rottura è stato efficacemente incrementato al 171%, mentre il modulo e il massimo stress sono risultati rispettivamente pari a 1734 MPa e 46 MPa. Nonostante la tenacità sia lievemente inferiore, il blend 50/40/10 rappresenta complessivamente una valida alternativa al blend 50/30/20 come materiale duttile.

Tabella II.VI Principali proprietà meccaniche del blend 50PLA/40PBS/10PHBH.

Modulo (MPa)	1734 ± 20
Deformazione al massimo stress (%)	4 ± 1
Massimo stress (MPa)	46 ± 1
Allungamento a rottura (%)	171 ± 14
Sforzo a rottura (MPa)	5 ± 1
Tenacità (J/m ³)	3417

III. Conclusioni

Il grafico in Figura III.I pone a confronto i blend studiati in base a lavorabilità, modulo, tenacità, allungamento a rottura, disponibilità e morfologia su una scala da 0 a 3, dove 3 è stato assegnato al blend che presenta il massimo livello relativo della caratteristica esaminata. I valori assegnati ai parametri derivano dai risultati della caratterizzazione dei blend, ad eccezione di lavorabilità e disponibilità. Le proprietà meccaniche sono state classificate eseguendo la proporzione tra i valori reali risultanti dalla caratterizzazione e la scala del grafico. La lavorabilità è stata intesa come la facilità con cui è avvenuto il processo di estrusione dei blend in termini di stabilità del flusso. Tutti i blend sono stati processati con lo stesso profilo vite e la medesima temperatura, tuttavia essi hanno richiesto un'attenzione diversa nella regolazione dei parametri di estrusione e di pelletizzazione, la quale è riflessa nei valori assegnati nel grafico. La disponibilità è stata valutata considerando le capacità produttive globali e il rapporto in peso di ciascun polimero

nei blend. Secondo European Bioplastics, la capacità produttiva dei poliidrossialcanoati (PHAs) è inferiore a quella di PLA e PBS. Inoltre, considerando che il PHBH rappresenta solo una piccola frazione della produzione dei PHAs, la quantità di biopolimero disponibile su base annua è scarsa; di conseguenza i blend a matrice PHBH sono meno disponibili rispetto a quelli a matrice PLA e hanno un valore inferiore assegnato nel grafico. Considerando il prezzo dei polimeri puri che è di circa 3 USD/kg per il PLA, 5 USD/kg per il PHBH e 6 USD/kg per il PBS e il loro rapporto in peso nei blend, si può presumere che l'andamento del prezzo dei blend abbia un andamento simile a quello della loro disponibilità. Tuttavia, poiché questo parametro è più difficile da quantificare rispetto agli altri, non è stato riportato nel grafico. Infine, la morfologia migliore, corrispondente al valore 3 nel grafico, è stata considerata quella avente dimensione minore delle fasi disperse e con la distribuzione più omogenea.

Osservando il grafico in Figura III.I è quindi possibile concludere che, i blend 50/40/10 e 50/30/20 presentano le caratteristiche complessivamente più equilibrate che li rendono adatti ad applicazioni in cui sono richiesti sia modulo che allungamento a rottura elevati. I blend contenenti maggiori quantità di PHBH invece, in particolare il 20/30/50, presentano la morfologia più fine e omogenea, ma proprietà meccaniche inferiori e il loro utilizzo è scoraggiato anche dalla ridotta disponibilità e lavorabilità.

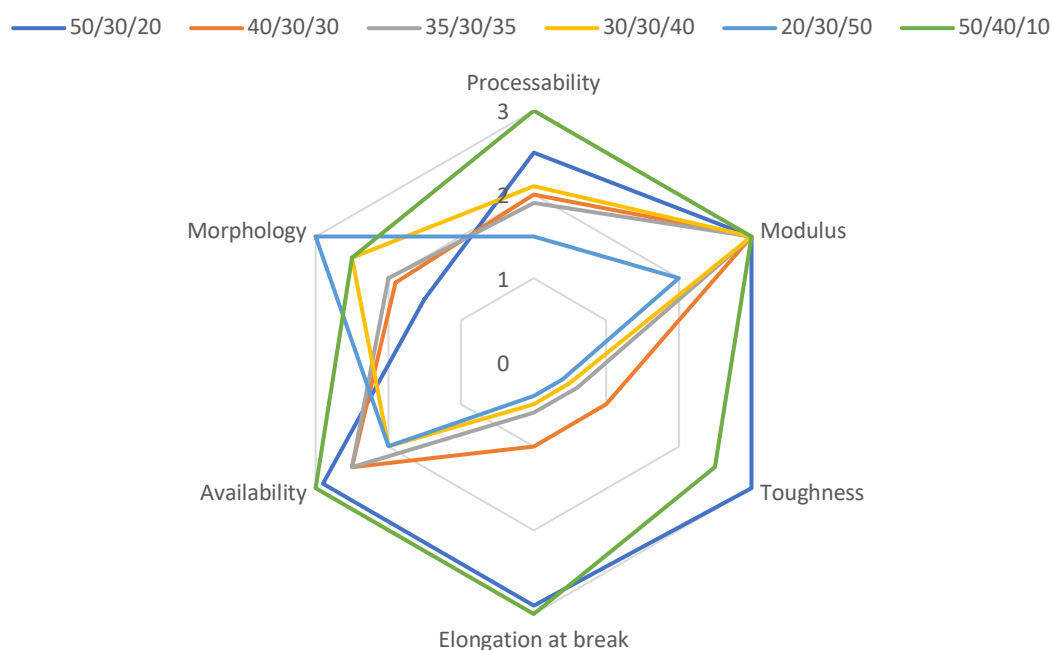


Figura 3.I Grafico radar di lavorabilità, modulo, tenacità, allungamento a rottura, disponibilità e morfologia dei blend.

List of figures

Figure 2.1 Schematic representation of morphologies forming in a ternary immiscible blends of polymer 1, 2 and 3 2. Reproduced from [11].....	3
Figure 2.2 Schematic diagram of the possible morphologies in a ternary blend composed of one major phase B and two minor phases A and C, as predicted by the spreading coefficients: a) A-phase encapsulated by C-phase, b) A and C form separated phases, c) C-phase encapsulated by A-phase and d) partial wetting morphology of polymers A and C. Modified from [12].....	5
Figure 2.3 Schematic diagram of the three possible phase structures when A is the matrix and B and C the dispersed phases for a ternary blend at equilibrium: a) structure B+C, b) structure B/C, c) structure C/B. Modified from [13].....	6
Figure 2.4 Stress-strain curves of neat PLA,PHBV and PLA/PHBV/PBS ternary blends. Reproduced from [15].	8
Figure 2.5 SEM images of blends A) PLA/PHBV/PBS 60/30/10; B) PLA/PHBV/PBS 60/10/30; C) PHBV/PLA/PBS 60/30/10; D) PHBV/PLA/PBS 60/10/30 and E) PHBV/PLA/PBS 60/30/10 with higher magnification. Reproduced from [15].....	9
Figure 2.6 Cooling DSC thermograms at cooling rate 20 °C/min for neat polymers and blends after melting at 190 °C for 3 min: A) PBS; B) PHBV; C) PLA; D) PLA/PHBV/PBS 60/30/10; E) PLA/PHBV/PBS 60/10/30; F) PHBV/PLA/PBS 60/30/10; G) PHBV/PLA/PBS 60/10/30. Reproduced from [15].	10
Figure 2.7 Second heating DSC thermograms after cooling 20 °C/min for neat polymers and blends: A) PBS; B) PHBV; C) PLA; D) PLA/PHBV/PBS 60/30/10; E) PLA/PHBV/PBS 60/10/30; F) PHBV/PLA/PBS 60/30/10; G) PHBV/PLA/PBS 60/10/30. Reproduced from [15].	10
Figure 2.8 FESEM images at different magnifications (left column x1000, right column x2000) of a), b) PLA/PHB/PBS blend and c), d) of PLA/PHB/PBSA blend. Reproduced from [16].	11
Figure 2.9 Frequency dependences of storage modulus G' (open symbols) and loss modulus G'' (closed symbols) for a) PLA and b) PBS. Reproduced from [17].	12
Figure 2.10 Frequency dependences of storage modulus G' (closed symbols) and loss modulus G'' (open symbols) for a) PLA/PBS 80/20; b) PLA/PBS 90/10 and c) PLA/PBS 95/5. Reproduced from [17].	12
Figure 2.11 a) G' curve as a function of frequency of PLA/PHB 70/30 and b) G'' slope (α) curve as a function of frequency of PLA/PHB 70/30 blend. Modified from [18].	13
Figure 3.1 Thermo Fisher Process 11 screw profile.....	16
Figure 3.2 Model Q20 TA Instruments calorimeter.....	17
Figure 3.3 Model ARES TA Instruments rheometer.	18
Figure 3.4 Model P 200 T Collin press.	19
Figure 3.5 Model 5966 Instron dynamometer.....	19
Figure 3.6 Model Babyplast 6/10P Cronoplast injection moulding machine.	20
Figure 4.1 Stress-strain curve of blend 50PLA/30PBAT/20PHBH compared to PLA, PBAT and PHBH.	24
Figure 4.2 Stress-strain curve of blend 50PLA/30PBSA/20PHBH compared to PLA, PBSA and PHBH.	25

Figure 4.3 Stress-strain curve of blend 50PLA/30PBS/20PHBH compared to PLA, PBS and PHBH.	26
Figure 4.4 Composition triangle of PLA/PBS/PHBH blends.	26
Figure 4.5 DSC cooling and second heating thermograms of neat polymers a) PLA b) PBS c) PHBH.	27
Figure 4.6 Cooling DSC thermograms of neat polymers and PLA/PBS/PHBH blends.	28
Figure 4.7 Second heating DSC thermograms of neat polymers and PLA/PBS/PHBH blends.	29
Figure 4.8 Complex viscosity curves as a function of frequency of neat polymers PLA, PBS and PHBH.	31
Figure 4.9 Complex viscosity curves as a function of frequency of the blends.	32
Figure 4.10 Storage modulus G' curve as a function of frequency of neat polymers PLA, PBS and PHBH.	33
Figure 4.11 Storage modulus G' curve as a function of frequency of the blends.	33
Figure 4.12 Han Chuang plot of the blends.	34
Figure 4.13 Van Gurp plot of the blends.	34
Figure 4.14 SEM images of cryo-fractured surface of 20/30/50 blend a) treated with acetic acid b) untreated.	35
Figure 4.15 SEM image of cryo-fractured surface of neat PHBH.	36
Figure 4.16 EDS spectrum of a platelet of 20/30/50 blend sample.	36
Figure 4.17 TGA analysis of neat PHBH sample.	37
Figure 4.18 SEM images of fracture-surfaces treated with acetic acid of the blends: a) 50/30/20, b) 40/30/30, c) 35/30/35, d) 30/30/40 and e) 20/30/50 at 5000x magnification.	38
Figure 4.19 Tensile stress-strain curves of PLA/PBS/PHBH blends.	39
Figure 5.1 Radar chart of processability, modulus, toughness, elongation at break, availability and morphology of the blends.	41

List of tables

Table 3.1 Code and composition of the studied blends.....	15
Table 3.2 Extrusion parameters for the blends.....	16
Table 3.3 Melting enthalpies of totally crystalline PLA, PHBH, PBAT, PBSA and PBS.	17
Table 3.4 Injection molding parameters for 50PLA/30PBAT/20PHBH, 50PLA/30PBSA/10PHBH, 50PLA/30PBS/20PHBH and 50PLA/40PBS/10PHBH blends... ..	20
Table 3.5 Injection molding parameters for 40PLA/30PBS/30PHBH, 35PLA/30PBS/35PHBH, 30PLA/30PBS/40PHBH and 20PLA/30PBS/50PHBH blends.....	21
Table 4.1 Main mechanical properties of pure polymers.....	23
Table 4.2 Mechanical properties of blend 50PLA/30PBAT/20PHBH.	23
Table 4.3 Mechanical properties of blend 50PLA/30PBSA/20PHBH.	24
Table 4.4 Mechanical properties of blend 50PLA/30PBS/20PHBH.	25
Table 4.5 Main thermal properties of neat polymers.	28
Table 4.6 Main thermal properties of PLA/PBS/PHBH blends.....	30
Table 4.7 Main mechanical properties of the PLA/PBS/PHBH blends.	40
Table 4.8 Toughness values of the PLA/PBS/PHBH blends.	40
Table 4.9 Main mechanical properties of 50PLA/40PBS/10PHBH blend.	40

1. Introduction

In recent years the effects of plastic pollution have become increasingly noticeable due to the accumulation of waste in natural environments, especially oceans and waterways; in fact, it has been estimated that of the 8.3 billion tons of plastics produced from 1950 to 2015, 4.9 billion tons were discarded into landfills or natural environments [1]. Plastics have a catastrophic effect on the natural environment by destroying habitats, strangling animals and being ingested by them leading to their death [2]. An increasing number of studies have proven that plastic pollution represents a risk for human health, due to the destruction of food chain and water supplies; furthermore, it allows the colonization and spreading of pathogens, dangerous microorganisms and harmful algal species [3]. Also plastic debris can be carriers of toxic additives or absorbed substances like bisphenol A, phthalates and heavy metals leading to endocrine disruption and oxidative stress causing cancer and accumulation along the food web [4]. Given all these serious threats to the environment and human health, the main actions aiming reducing plastic pollution are to reduce the production and use of plastics, to improve the management and collection of plastic waste, to optimize the technologies concerning plastic production and recycling and to increase the use of sustainable bioplastics.

According to European Bioplastics Organization, a bioplastic is a plastic material that is either biodegradable, biobased or both [5]. So, a bioplastic can belong to three different plastic categories: fossil-based biodegradable plastics (PBAT, PCL), biobased non-biodegradable plastics (Bio-PE, Bio-PET) and biobased biodegradable plastics (PLA, PHA), the latter being considered as “true bioplastics” because they join the advantages of deriving from biomass to the ability to biodegrade at their end of use [6]. Bioplastics are considered to be more sustainable than traditional polymers, because they reduce the amount of fossil fuels used for their production, they can derive from agricultural products that otherwise would be wasted and at their end of life they can be biodegraded by microorganism thus reducing the plastic pollution problem. However, there are some drawbacks associated with the use of bioplastics, as their disposal is not always easy because biodegradation takes a long time and requires a controlled composting environment. To produce bio-based bioplastic, the raw materials are usually food feedstock; therefore, there is a competition between the use of land for food or technology. Lastly, their physical, mechanical and chemical properties are typically lower compared to those of fossil fuel-based plastics. Additionally, another important downside is the high cost of bioplastics, which severely limits their diffusion [7] [8]. Polylactic acid (PLA) is one of the most used biopolymers up to date, having properties comparable to many of traditional thermoplastic polymers, however its main disadvantage is its brittleness, which limits some of applications. To overcome these limitations, it is possible to formulate PLA-based blends with different polymers to engineer its properties and expand the applications field.

The first chapter of this work deals with the thermodynamic principles involved in the blends, the influence of interfacial forces on morphologies and the existing research background concerning ternary blends. The second chapter describes the materials and methods used for the production and characterization of ternary biopolymer blends based on polylactic acid (PLA) and polyhydroxy butyrate-co-hexanoate (PHBH) with the addition of either polybutylene adipate-co-terephthalate (PBAT), polybutylene succinate-co-adipate (PBSA) or polybutylene succinate (PBS). Subsequently, in the third chapter, there is the description of the selection process of the blends composition, followed by the description and discussion of the results of characterizations of the different blend formulations.

2. Ternary blends

Polymeric blends are mixtures of two or more polymers in which the components may be thermoplastics, thermosets or elastomers below or above their glass or melt temperatures. They may have properties similar to one of the components, weighted averages or show synergism [9]. Blends are engineered to obtain materials with optimized structural, mechanical, morphological, chemical and biological properties which are determined by the type and distribution of the components, as well as the type, shape and size distribution of structures formed by one polymer in the other. They have several advantages, filling the economical and performance gaps of pure polymers, being an economically viable and versatile way for tailoring new specific materials and enabling maximization of properties through engineering of type and combination of components.

Polymer blends are classified as miscible and immiscible, the latter being the most common type. Miscibility is determined by thermodynamics through Gibbs free energy of mixing which must be negative for two polymers to be miscible. Flory-Huggins theory, which is a mathematical model able to explain the thermodynamics of polymer solutions, can be extended to ternary polymeric blends as it will be described in the following sections.

As mentioned above, the majority of polymer-based blends is immiscible, and in ternary immiscible blend where two phases are dispersed in a continuous major phase, the formation of the two dispersed phases in the matrix, as well as the size of dispersed particle are crucial factors affecting their performance. So, by controlling morphology it is possible to vary several blends properties, starting from the mechanical ones. Considering a ternary blend of polymer 1, polymer 2 and polymer 3 where polymer 3 is the continuous matrix, three phase formations are expected, as shown schematically in Figure 2.1: a) capsule formation with polymer 2 encapsulated by polymer 1, b) stack formation of polymers 1 and 2 stuck together and c) isolated formation with polymers 1 and 2 dispersed separately in polymer 3 matrix. The development of morphology in this kind of blends is governed mostly by the interfacial tensions between each component as explained by Hobbs et al. [10] and later discussed in Section 2.3 [11].

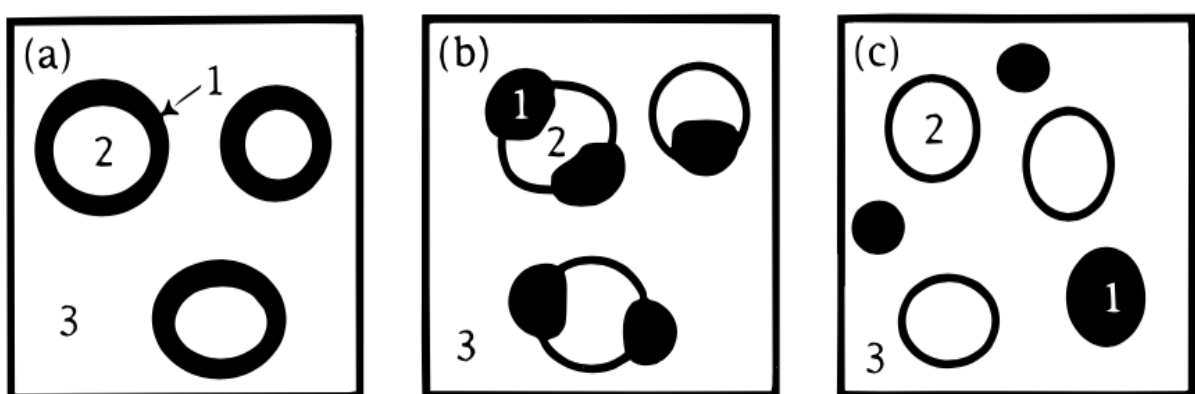


Figure 2.1 Schematic representation of morphologies forming in a ternary immiscible blends of polymer 1, 2 and 3. Reproduced from [11].

2.1 Thermodynamics of polymeric blends

The Gibbs free energy of mixing can be expressed as a function of enthalpy and entropy of mixing according to the equation:

$$\Delta G_{mix} = \Delta H_{mix} - T\Delta S_{mix} \quad (2.1)$$

where ΔH_{mix} and ΔS_{mix} are the enthalpic and entropic contributions, respectively. The competition between these two contributions determines the Gibbs free energy of mixing; in fact, if $\Delta G_{mix} < 0$ spontaneous mixing of the polymers occurs, while if $\Delta G_{mix} > 0$ the polymers do not mix, and the system is incompatible.

For high molecular weight polymers, the entropic contribution ΔS_{mix} is negligible and in most cases ΔH_{mix} is positive, so most of polymer combinations are immiscible unless there are favourable specific interaction between them such as hydrogen bonds or dipole-dipole interactions. Immiscibility leads to a heterogeneous structure in which the domain size and final morphology are governed by phase-separation thermodynamics and interfacial properties of the blend components [11].

2.2 Flory-Huggins theory

Flory-Huggins theory is a relatively simple thermodynamic model for polymer-polymer blends that express the Gibbs free energy of mixing as a function of an interaction parameter precisely called Flory-Huggins interaction parameter. The theory leads to the conclusion that to have miscible blends in the limit of high molecular weights the interaction parameter has to be negative. For a ternary blend the Flory-Huggins equation can be expressed as:

$$\begin{aligned} \frac{\Delta G_{mix}}{kT} = & \frac{\phi_1}{N_1 v_1} \ln \phi_1 + \frac{\phi_2}{N_2 v_2} \ln \phi_2 + \frac{\phi_3}{N_3 v_3} \ln \phi_3 + \frac{\phi_1 \phi_2}{v_{12}} \chi_{12}^{FH} \\ & + \frac{\phi_1 \phi_3}{v_{13}} \chi_{13}^{FH} + \frac{\phi_2 \phi_3}{v_{23}} \chi_{23}^{FH} \end{aligned} \quad (2.2)$$

where ΔG_{mix} is the Gibbs free energy of mixing per unit volume, k is Boltzmann's constant, T is the absolute temperature, ϕ_i is the volume fraction of component i , N_i is the number of segments per molecule of component i , v_i is the average segmental volume of component i and χ_{ij}^{FH} is the Flory-Huggins interaction parameter between component i and j . This parameter can also be related to the solubility parameters of two components by the equation:

$$\chi = \frac{V}{RT} (\delta_1 - \delta_2)^2 \quad (2.3)$$

where V is the volume of the probe and δ_1 and δ_2 are the solubility parameters of the polymer and polymer stationary phase respectively. Given the fact that the difference between these two quantities is squared, the equation implies that χ is always positive and so ΔG_{mix} . A negative value of χ and thus a negative ΔG_{mix} can only occur in systems in which specific interactions are present [11].

2.3 Effect of interfacial forces on blend morphologies

A prediction of the phase structures forming in a multi-component system has been proposed by Hobbs et al. [10] who have rewritten Harkin's equation for a ternary system in which A is the continuous phase with B and C as the dispersed phases. For this type of system, the spreading coefficient of the B-phase on the C-phase is:

$$\lambda_{BC} = \gamma_{AC} - \gamma_{AB} - \gamma_{BC} \quad (2.4)$$

where γ_{ij} is the interfacial tension between i and j phases. According to Hobbs et al. if the spreading coefficient λ_{BC} is positive, B-phase encapsulates C-phase. Similarly, if the spreading coefficient of the C-phase on the B-phase expressed by the equation:

$$\lambda_{CB} = \gamma_{AB} - \gamma_{AC} - \gamma_{BC} \quad (2.5)$$

is positive, C-phase encapsulates B-phase. Conversely, if both λ_{BC} and λ_{CB} are negative, B-phase and C-phase remain separate.

Figure 2.2 summarizes the spreading coefficients corresponding to the possible morphologies occurring in a ternary blend with one continuous phase. Figure 2.2 a, b and c show three possible morphologies corresponding to complete wetting, in which one minor phase shares its area with just one of the other phases. Complete wetting can take one of two forms: two separate droplets (Figure 2.2 b) or core-shell structure (Figure 2.2 a, c), in each case one of the spreading coefficients is positive while the others are negative. Figure 2.2 d shows the fourth possibility in which the three spreading coefficients are all negative, in that case each polymer phase is adjacent to the other two and shares its surface area with both the other components.

	<p>a)</p> $\lambda_{ABC} = \gamma_{AC} - \gamma_{AB} - \gamma_{BC} < 0$ $\lambda_{ACB} = \gamma_{AB} - \gamma_{AC} - \gamma_{BC} > 0$ $\lambda_{BAC} = \gamma_{BC} - \gamma_{AB} - \gamma_{AC} < 0$		<p>b)</p> $\lambda_{ABC} = \gamma_{AC} - \gamma_{AB} - \gamma_{BC} > 0$ $\lambda_{ACB} = \gamma_{AB} - \gamma_{AC} - \gamma_{BC} < 0$ $\lambda_{BAC} = \gamma_{BC} - \gamma_{AB} - \gamma_{AC} < 0$
	<p>c)</p> $\lambda_{ABC} = \gamma_{AC} - \gamma_{AB} - \gamma_{BC} < 0$ $\lambda_{ACB} = \gamma_{AB} - \gamma_{AC} - \gamma_{BC} < 0$ $\lambda_{BAC} = \gamma_{BC} - \gamma_{AB} - \gamma_{AC} > 0$		<p>d)</p> $\lambda_{ABC} = \gamma_{AC} - \gamma_{AB} - \gamma_{BC} < 0$ $\lambda_{ACB} = \gamma_{AB} - \gamma_{AC} - \gamma_{BC} < 0$ $\lambda_{BAC} = \gamma_{BC} - \gamma_{AB} - \gamma_{AC} < 0$

Figure 2.2 Schematic diagram of the possible morphologies in a ternary blend composed of one major phase B and two minor phases A and C, as predicted by the spreading coefficients: a) A-phase encapsulated by C-phase, b) A and C form separated phases, c) C-phase encapsulated by A-phase and d) partial wetting morphology of polymers A and C. Modified from [12].

Even though this model allows correct prediction of many morphologies, it does not consider interfacial free energy, which is a combination of interfacial tensions and interfacial areas, so it has been modified by Guo et al. [13].

The model proposed by Guo et al. is based on the concept that phase morphology of a multicomponent polymer system will be that which has the lowest free energy. For a multiphase polymer system, the Gibbs free energy can be written as:

$$G = \sum_i n_i \mu_i + \sum_{i \neq j} A_i \gamma_{ij} \quad (2.6)$$

where n is the number of moles, μ is the chemical potential, A is the interfacial area and γ is the interfacial tension. For a N -component system ($N > 2$) the number of possible interfaces is:

$$m = \frac{N!}{2!(N-2)!} \quad (2.7)$$

However, since only $N - 1$ interfaces can coexist in the system at the lowest free energy, the number of different possible phase structure is given by the following equation:

$$q = N \left\{ \frac{m!}{(N-1)! [m - (N-1)]!} - \frac{N [m - (N-1)]!}{(N-1)! [m - 2(N-1)]!} \right\} \quad (2.8)$$

Considering a ternary blend, there are two coexisting interfaces and nine possible phase structures. Figure 2.3 shows a schematic representation of the three possible phase structures when A is the continuous phase and B and C are the dispersed phase a) B and C form separated phases (B+C); b) C-phase is encapsulated by B-phase (B/C) and c) B-phase is encapsulated by C-phase (C/B). The other six possible phase structure are analogous but with B or C as the continuous phase.

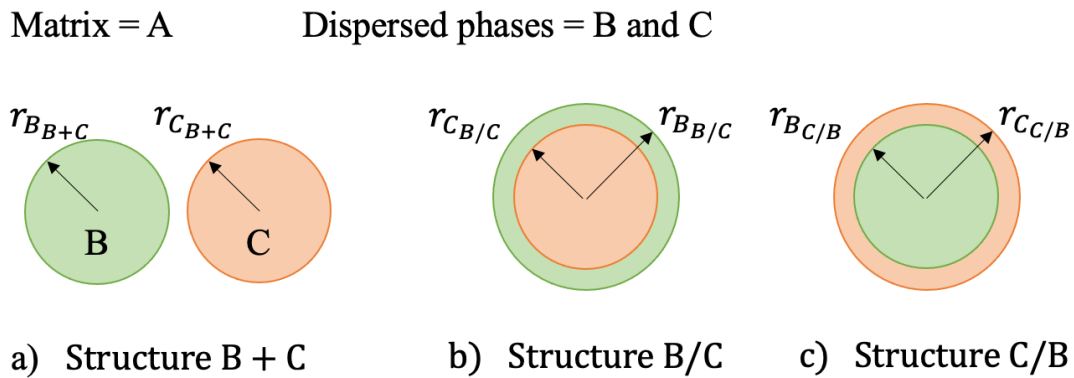


Figure 2.3 Schematic diagram of the three possible phase structures when A is the matrix and B and C the dispersed phases for a ternary blend at equilibrium: a) structure B+C, b) structure B/C, c) structure C/B. Modified from [13].

The Gibbs free energy for each structure in figure is:

$$\begin{aligned}
\text{a)} \quad G_{B+C} &= (n_1\mu_1 + n_2\mu_2 + n_3\mu_3) + (A_{B_{B+C}}\gamma_{AB} + A_{C_{B+C}}\gamma_{AC}) \\
\text{b)} \quad G_{B/C} &= (n_1\mu_1 + n_2\mu_2 + n_3\mu_3) + (A_{B_{B/C}}\gamma_{AB} + A_{C_{B/C}}\gamma_{BC}) \\
\text{c)} \quad G_{C/B} &= (n_1\mu_1 + n_2\mu_2 + n_3\mu_3) + (A_{B_{C/B}}\gamma_{BC} + A_{C_{C/B}}\gamma_{AC})
\end{aligned} \tag{2.9}$$

And the surface areas of B-phase and C-phase in the three structures are:

$$\begin{aligned}
A_{B_{B+C}} &= 3V \sum \frac{\phi_{B^i}}{r_{B_{B+C}^i}} & A_{C_{B/C}} &= 3V \sum \frac{\phi_{C^i}}{r_{C_{B/C}^i}} \\
A_{C_{B+C}} &= 3V \sum \frac{\phi_{C^i}}{r_{C_{B+C}^i}} & A_{B_{C/B}} &= 3V \sum \frac{\phi_{B^i}}{r_{B_{C/B}^i}} \\
A_{B_{B/C}} &= 3V \sum \frac{\phi_{B^i} + \phi_{C^i}}{r_{B_{B/C}^i}} & A_{C_{C/B}} &= 3V \sum \frac{\phi_{B^i} + \phi_{C^i}}{r_{C_{C/B}^i}}
\end{aligned} \tag{2.10}$$

where V is the total volume, ϕ_B and ϕ_C are the volume fractions of B-phase and C-phase and r_{B+C} , $r_{B/C}$ and $r_{C/B}$ are the radii of dispersed phase in the three structure as shown in Figure 2.2.

The phase structure of a ternary polymer blend can then be predicted by comparing the Gibbs free energies of the different structures. Because the $n_i\mu_i$ terms of equation 2.9 are the same for each structure they can be neglected and to further simplify the problem, the areas A_B and A_C of the minor phases can be calculated based on average phase sizes. The interfacial free energies for different phase structures can be calculated as:

$$\begin{aligned}
(\Sigma A_i \gamma_{ij})_{B+C} &= (4\pi)^{1/3} (n_B^{1/3} x^{2/3} \gamma_{AB} + n_C^{1/3} \gamma_{AC}) (3V_C)^{2/3} \\
(\Sigma A_i \gamma_{ij})_{B/C} &= (4\pi)^{1/3} (n_B^{1/3} (1+x)^{2/3} \gamma_{AB} + n_C^{1/3} \gamma_{BC}) (3V_C)^{2/3} \\
(\Sigma A_i \gamma_{ij})_{C/B} &= (4\pi)^{1/3} (n_B^{1/3} x^{2/3} \gamma_{BC} + n_C^{1/3} (1+x)^{2/3} \gamma_{AC}) (3V_C)^{2/3}
\end{aligned} \tag{2.11}$$

where $x = V_B/V_C$, n_B and n_C are the number of particles of B-phase and C-phase. Hence the values of $\Sigma A_i \gamma_{ij}$ can be compared for the three structures and the lowest value will correspond to the equilibrium phase structure of the system. It must be noted that this model assumed for simplicity that the number of B and C particles is the same ($n_B = n_C$) which may not be true in practice, however, given the fact that the total surface area of a dispersed phase depends on the cubic root of the particle number, the relative interfacial energies of different phase structures are not very sensitive to the particle numbers of the minor phases [13].

2.4 Background of PLA-based ternary blends

Research concerning PLA-based biopolymeric blends is a sector in constant growth in recent years, as they are viable alternatives to traditional petroleum-based polymers in engineering and commodity applications. PLA is often the base material because it is characterized by high modulus, good barrier properties, high strength, competitive material and processing costs, biocompatibility and biodegradability. Nevertheless its brittleness, very low toughness,

sometimes problematic processability and low service temperatures are the main limitations that blending attempts to overcome [14]. Even though research is growing, it is quite limited regarding ternary blends, in particular containing polymers studied in this work PHBH, PBSA, PBAT and PBS.

The research of Zhang et al. [15] focused on mechanical, thermal and morphological analyses of PLA/PHBV/PBS blends with different compositions. As shown in Figure 2.4 neat PLA and neat PHBV (poly hydroxybutyrate-co-hydroxyvalerate) are quite rigid and there is no obvious yield observed from the stress-strain curves; on the other hand, all ternary blends show excellent balance in tensile properties and they all exhibit distinct yielding and cold drawing, which are indicators of a transition from brittle-to-ductile fracture.

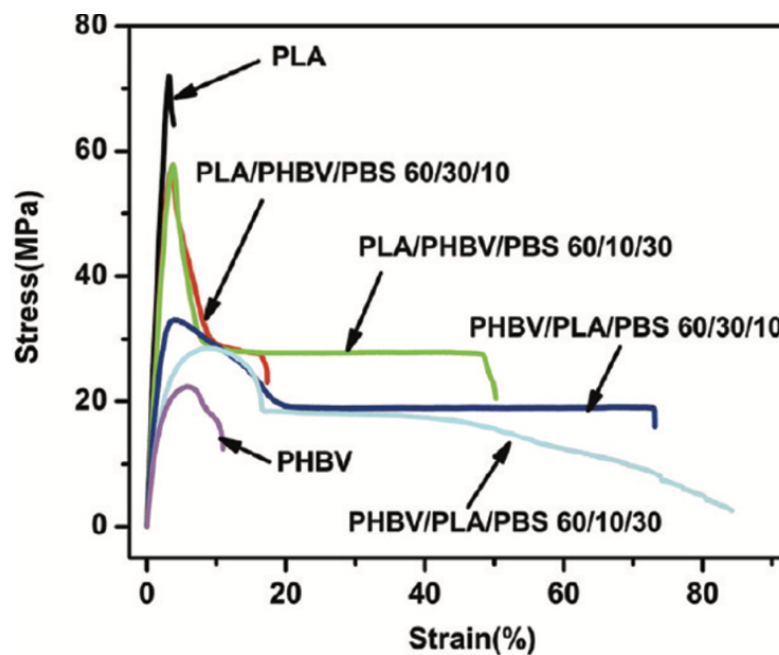


Figure 2.4 Stress-strain curves of neat PLA, PHBV and PLA/PHBV/PBS ternary blends. Reproduced from [15].

Considering the elongation at break which is around 4% and 10% for neat PLA and neat PHBV respectively, the PLA/PHBV/PBS 60/30/10 and PLA/PHBV/PBS 60/10/30 blends reached around 23% and 50%, respectively while PHBV/PLA/PBS 60/30/10 and PHBV/PLA/PBS 60/10/30 reached around 64% and 82%, respectively. These results demonstrated that the higher the amount of PBS, the higher is the elongation at break and with the same amount of PBS a higher PHBV content leads to higher elongation. As expected, the tensile modulus of the blends decreased by increasing PHBV and PBS content due to the incorporation of a soft phase in the PLA matrix.

The morphology was studied by Zhang et al. with a scanning electron microscope (SEM), as shown in Figure 2.5, it is possible to observe PHBV and PBS particles and dark holes left by them during fracture. These phases are dispersed as spheres in the continuous PLA or PHBV matrix and their surface is smooth with clean borders, suggesting poor compatibility and weak interfacial adhesion between the phases. The only exception is PHBV/PLA/PBS 60/30/10 blend which shows a typical core-shell morphology with PLA encapsulating PBS. These results are coherent with the λ_{13} values calculated with Hobbs et al. prediction model, in fact λ_{13} is negative for all the blends except PHBV/PLA/PBS 60/30/10, which has a positive value.

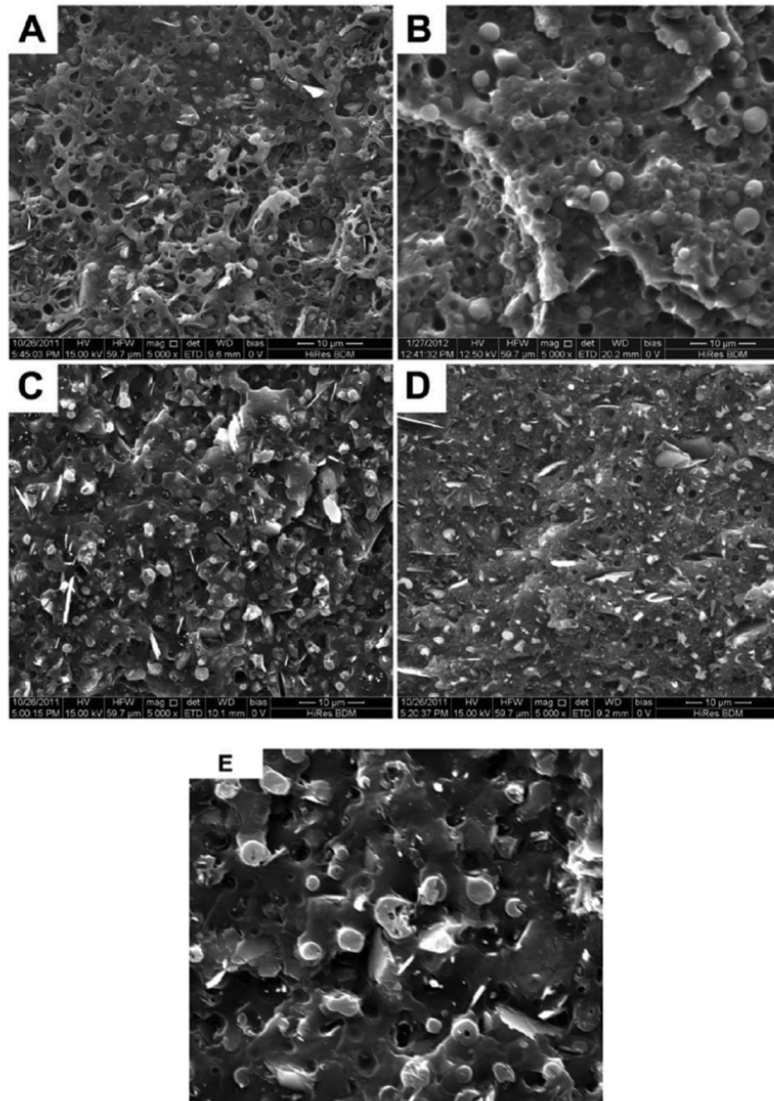


Figure 2.5 SEM images of blends A) PLA/PHBV/PBS 60/30/10; B) PLA/PHBV/PBS 60/10/30; C) PHBV/PLA/PBS 60/30/10; D) PHBV/PLA/PBS 60/10/30 and E) PHBV/PLA/PBS 60/30/10 with higher magnification. Reproduced from [15].

Concerning the thermal characterization of the blends, by looking at the cooling thermogram deriving from the DSC analysis in Figure 2.6 and comparing the curves of the blends to neat polymers, the crystallization temperature of PHBV shifted to lower temperature indicating that its crystallization is restricted by PLA and PBS phases which suppressed the nucleation of PHBV in the blends. On the contrary the crystallization temperature of PBS shifted to higher temperature, indicating that its crystallization is promoted in the blends.

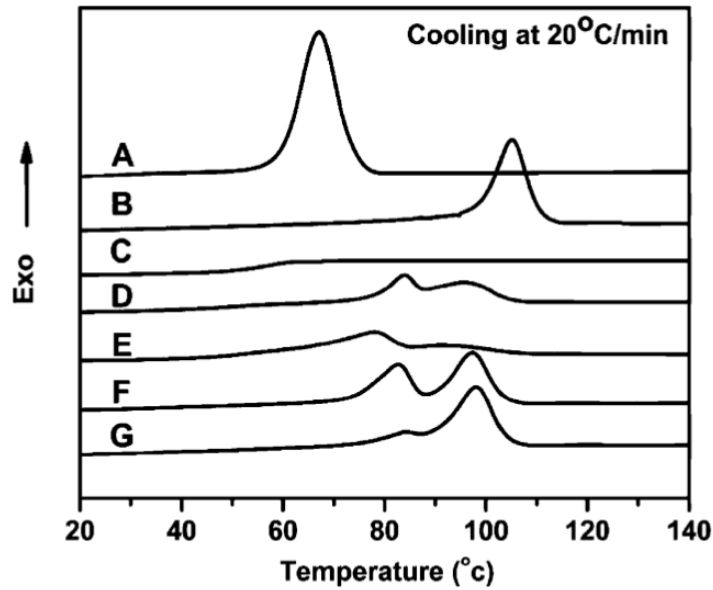


Figure 2.6 Cooling DSC thermograms at cooling rate 20 °C/min for neat polymers and blends after melting at 190 °C for 3 min: A) PBS; B) PHBV; C) PLA; D) PLA/PHBV/PBS 60/30/10; E) PLA/PHBV/PBS 60/10/30; F) PHBV/PLA/PBS 60/30/10; G) PHBV/PLA/PBS 60/10/30. Reproduced from [15].

Also, the second heating thermogram in Figure 2.7 showed that the cold crystallization temperature of PLA in the blends shifted to lower temperature, which indicates that cold crystallization of PLA is promoted by the addition of PHBV and PBS. The observed enhancement of cold crystallization can be attributed to the activation of PLA chain mobility by the amorphous phases of PHBV and PBSA and to the surface of PHBV and PBS that might act as nucleating center for PLA. These variations in crystallinity partially determine the mechanical properties possessed by the blends.

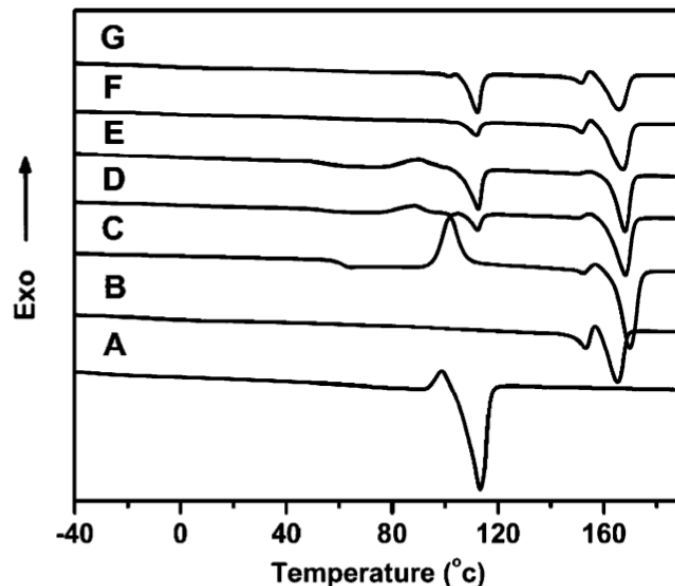


Figure 2.7 Second heating DSC thermograms after cooling 20 °C/min for neat polymers and blends: A) PBS; B) PHBV; C) PLA; D) PLA/PHBV/PBS 60/30/10; E) PLA/PHBV/PBS 60/10/30; F) PHBV/PLA/PBS 60/30/10; G) PHBV/PLA/PBS 60/10/30. Reproduced from [15].

Garcia-Campo et al. [16] studied the mechanical and morphological behaviour of 60 PLA/10 PHB/30 PBS and 60 PLA/10 PHB/30 PBSA. Compared to neat PLA, PBS and PBSA resulted to have a positive effect on elongation at break (7.6% for neat PLA) and the ternary blends PLA/PHB/PBS and PLA/PHB/PBSA showed values up to 49.3% and 62.9% respectively. On the other hand, as expected the tensile strength and modulus decreased in the ternary blends. Compared to neat PLA which had 3514 MPa modulus and 57.6 MPa tensile strength, PLA/PHB/PBS blend showed 1902 MPa modulus and 49.3 MPa tensile strength and PLA/PHB/PBSA blend just 1715 MPa modulus and 42.7 MPa tensile strength.

Concerning the blends morphology, the FESEM images of the PLA/PHB/PBS blend reported in Figure 2.8 a, b showed clear phase separation indicating poor miscibility, also a gap could be detected between the PLA-rich phase and the dispersed spherical domains which once again is an indicator of poor miscibility of the phases. From the images referring to PLA/PHB/PBSA blend in Figure 2.8 c, d a different morphology is observed, as the spherical domains are lower in size compared to the other blend, and that could be related to the higher ductility of PBSA compared to PBS.

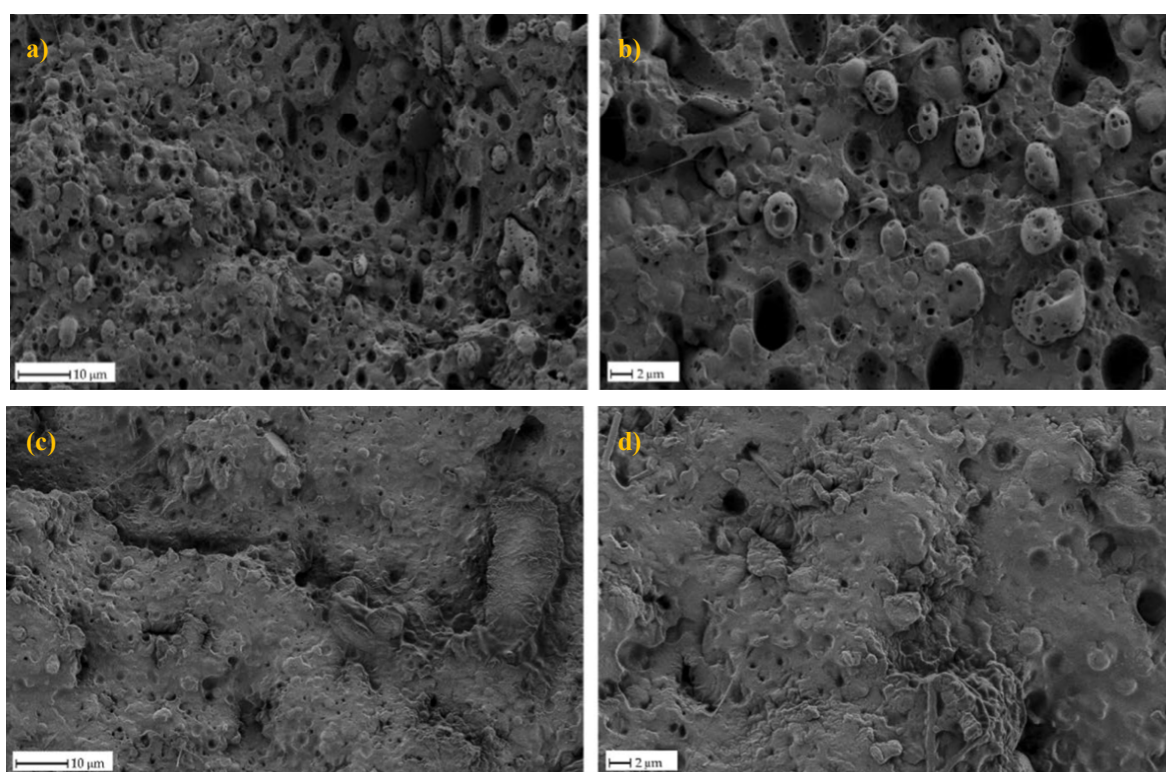


Figure 2.8 FESEM images at different magnifications (left column x1000, right column x2000) of a), b) PLA/PHB/PBS blend and c), d) of PLA/PHB/PBSA blend. Reproduced from [16].

As previously stated, the existing literature concerning these types of ternary biopolymer blends is scarce, especially about rheological measures. Nevertheless, there is some information regarding binary biopolymer blends; in this context, Yokohara et al. [17] studied the rheological behaviour of a PLA/PBS binary blend. The measurements showed that the blend had a different rheological behaviour compared to neat polymers, as both PLA and PBS moduli G'' and G' exhibited slopes of 1 and 2 respectively at low frequencies (Figure 2.9).

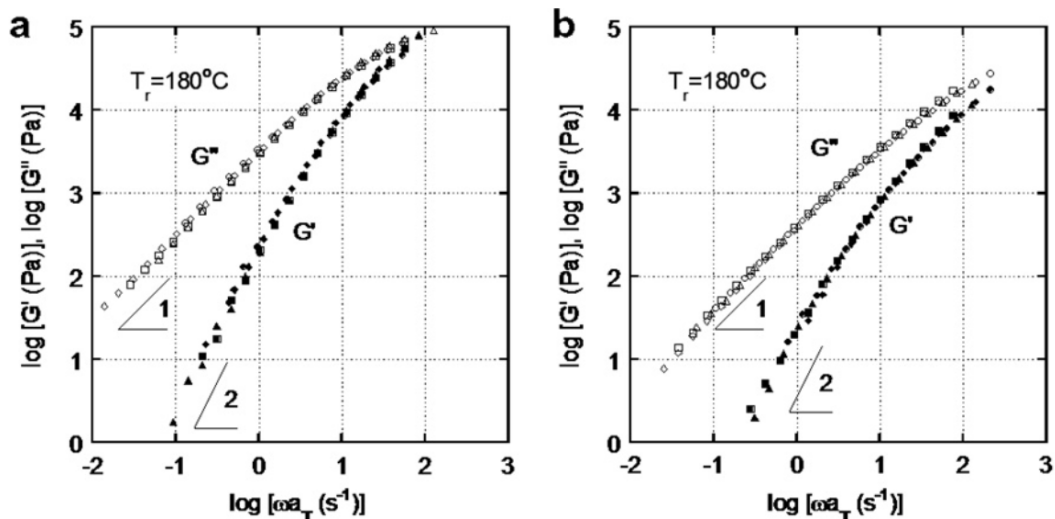


Figure 2.9 Frequency dependences of storage modulus G' (open symbols) and loss modulus G'' (closed symbols) for a) PLA and b) PBS. Reproduced from [17].

Observing the frequency dependences of the moduli G' and G'' of the PLA/PBSA blends reported in Figure 2.10 it is possible to recognize different behaviors, since G' curve exhibit a shoulder in the low frequency region as PBS content increases. The observed shoulder peak suggests there is a long-time relaxation mechanism which is related to the recovery process from the deformed state of the dispersed phase that in turn is related to the interfacial tension between the continuous and dispersed phases.

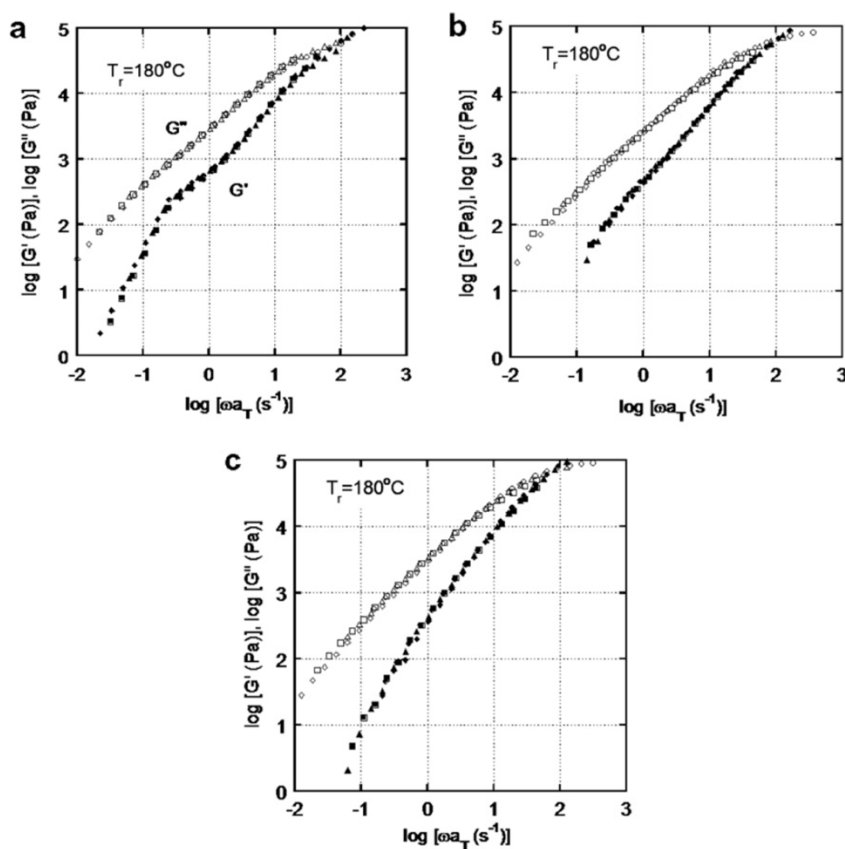


Figure 2.10 Frequency dependences of storage modulus G' (closed symbols) and loss modulus G'' (open symbols) for a) PLA/PBS 80/20; b) PLA/PBS 90/10 and c) PLA/PBS 95/5. Reproduced from [17].

D'Anna et al. [18] studied the rheological behavior of a PLA/PHB 70/30 blend. Figure 2.11a shows the blend storage modulus G' curve as a function of the frequency, which exhibits a shoulder peak in the low frequency region that can be related to the recovery process of the dispersed phase, and it is typical of immiscible blends. The curve of G' slope (α) as a function of frequency of the blend reported in Figure 2.11b shows a progressive decrease as the frequency increases, associable to the continuous relaxation of the droplets constituting the dispersed phase.

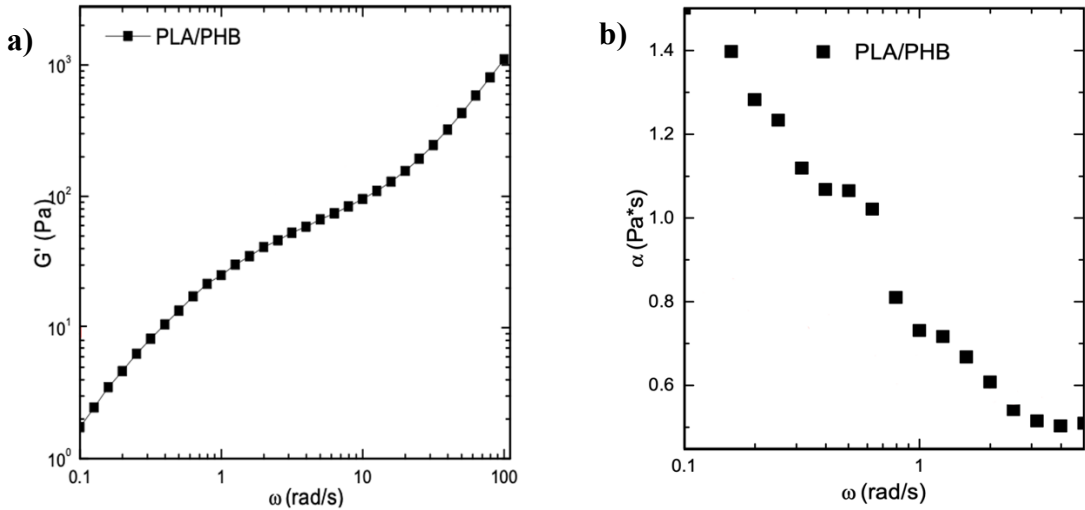


Figure 2.11 a) G' curve as a function of frequency of PLA/PHB 70/30 and b) G' slope (α) curve as a function of frequency of PLA/PHB 70/30 blend. Modified from [18].

3. Materials and methods

3.1 Materials

All biopolymers were supplied in form of pellets.

PLA was supplied by Ingeo™ Natural Natureworks under the trade name PLA3251D, with the following main properties: density=1.24 g/cm³, MFI=33 g/10min (210°C, 2.16 kg).

PHBH was supplied by Maip under the trade name IamNature B6A13, with the following main properties: density 1.20 g/cm³, MFI=7 g/10min (165 °C, 5 kg).

PBAT was supplied by Maip under the trade name Orios B7T T108HT, with the following main properties: density 1.25 g/cm³, MFR=4 g/10min (190 °C, 2.16 kg).

PBSA was supplied by Maip under the trade name Orios B7 M 29DF, with the following main properties: density 1.24 g/cm³, MFR=4 g/10min (190 °C, 2.16 kg).

PBS was supplied by Natureplast under the trade name PBE003, with the following main properties: density 1.26 g/cm³, MFR=4-6 g/10min (190 °C, 2.16 kg).

3.2 Blend preparation

The preparation of blends started from the extrusion of PLA with a co-rotating twin screw Leistritz ZSE extruder in order to obtain smaller pellets, which could be more readily processed during the blend compounding.

Neat polymers pellets were weighted according to the chosen composition of blends reported in Table 3.1 and manually mixed. The obtained mixed pellets were then dried overnight at 70 °C for about 8 hours in a Piovani HR50 oven to remove any retained moisture.

Table 3.1 Code and composition of the studied blends.

Code	Composition (%wt.)
50PLA/30PBAT/20PHBH	PLA: 50%; PBAT: 30%; PHBH: 20%
50PLA/30PBSA/20PHBH	PLA: 50%; PBSA: 30%; PHBH: 20%
50PLA/30PBS/20PHBH	PLA: 50%; PBS: 30%; PHBH: 20%
50PLA/40PBS/10PHBH	PLA: 50%; PBS: 40%; PHBH: 10%
40PLA/30PBS/30PHBH	PLA: 40%; PBS: 30%; PHBH: 30%
35PLA/30PBS/35PHBH	PLA: 35%; PBS: 30%; PHBH: 35%
30PLA/30PBS/40PHBH	PLA: 30%; PBS: 30%; PHBH: 40%
20PLA/30PBS/50PHBH	PLA: 20%; PBS: 30%; PHBH: 50%

The blends were then prepared using a parallel twin screw Thermo Fisher Scientific Process 11 extruder, characterized by diameter $\Phi = 11\text{mm}$ and L/D ratio = 40. The used screw profile

reported in Figure 3.1 is a standard type with three mixing sections. The process parameters that allowed good flow stabilization were different for each blend as reported in Table 3.2. After the extrusion, the extrudate was submerged in a water bath and pelletized.

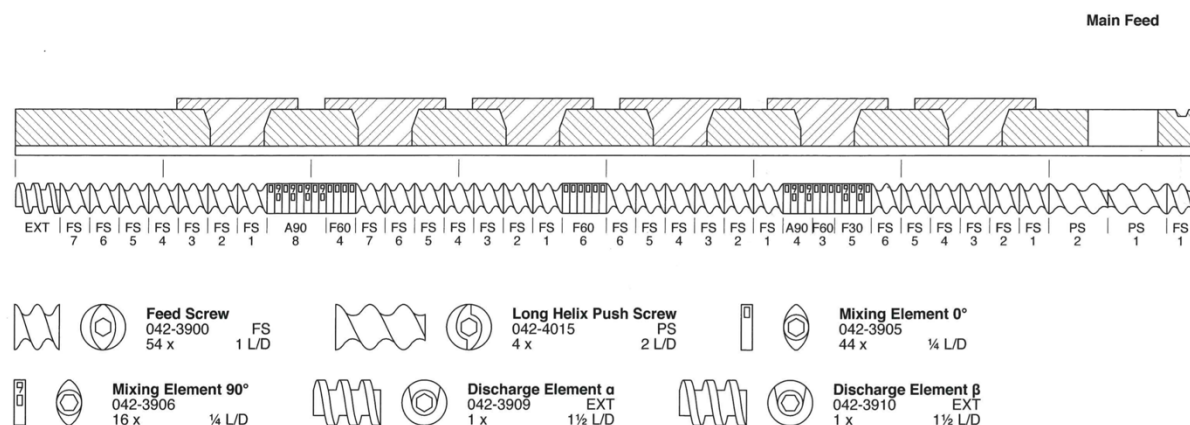


Figure 3.1 Thermo Fisher Process 11 screw profile.

Table 3.2 Extrusion parameters for the blends.

Blend	Barrel temperature (°C)	Feed rate (g/hour)	Screw speed (rpm)	Melt temperature (°C)	Pressure (bar)	Torque (%)
50PLA/30PBAT	120/175/175/175/	460	350	158	11	37
/20PHBH	175/175/175/175					
50PLA/30PBSA	100/170/170/170/	470	350	165	8	35
/20PHBH	165/165/165/165					
50PLA/30PBS	100/170/170/170/	380	250	155	19	44
/20PHBH	165/165/165/165					
50PLA/40PBS	100/170/170/170/	1020	280	155	19	52
/10PHBH	165/165/165/165					
40PLA/30PBS	100/170/170/170/	700	250	156	27	45
/30PHBH	165/165/165/165					
35PLA/30PBS	100/170/170/170/	630	250	157	19	40
/35PHBH	165/165/165/165					
30PLA/30PBS	100/170/170/170/	680	230	153	17	44
/40PHBH	165/165/165/165					
20PLA/30PBS	100/170/170/170/	740	300	161	22	40
/50PHBH	165/165/165/165					

3.3 Characterization techniques

3.3.1 Differential Scanning Calorimetry (DSC)

DSC analysis was performed using a Q20 TA Instruments (New Castle, DE, USA) calorimeter (Figure 3.2). The tests were carried out on a single pellet of about 7 mg. To remove the thermal history of the materials associated with processing, the samples were subjected to the following heating cycle: heating from -50 to 200 °C, cooling from 200 to -50 °C and a second heating from -50 to 200 °C; the scanning rate was maintained during the whole cycle at 10 °C/min. Glass transition temperature T_g , melting temperature T_m , crystallization temperature T_c and cold crystallization temperature T_{cc} and the enthalpy values associated with each thermal event were determined from the analysis. The crystallinity percentage of samples was evaluated using the following formula:

$$\chi (\%) = \frac{\Delta H}{\Delta H^0} \cdot 100 \quad (3.1)$$

where $\Delta H = \Delta H_m - \Delta H_{cc}$ (being ΔH_m melting enthalpy and ΔH_{cc} cold crystallization enthalpy) and ΔH^0 is the melting enthalpy of the totally crystalline polymer measured at the equilibrium melting point, which is reported in Table 3.3 for used biopolymers.



Figure 3.2 Model Q20 TA Instruments calorimeter.

Table 3.3 Melting enthalpies of totally crystalline PLA, PHBH, PBAT, PBSA and PBS.

Polymer	ΔH^0 (J/g)
PLA	93.6 [19]
PHBH	146 [20]
PBAT	114 [21]
PBSA	116.9 [22]
PBS	110.5 [23]

3.3.2 Rheological measurements

Rheological measurements were performed using an ARES TA Instrument (New Castle, USA) parallel plate rheometer (Figure 3.3), with plate diameter of 25 mm. The tests were carried out with a 1 mm gap between the plates, at 180 °C in nitrogen atmosphere to avoid polymer degradation by oxidation. Two different experiments were performed:

- Strain sweep tests at 100 rad/s frequency and 0.1-100% deformation in order to detect the limit of the linear viscoelastic region which resulted to be 20% for every blend.
- Frequency sweep tests at 0.1-100 rad/s frequency and 20% of strain amplitude to measure complex viscosity η^* , storage modulus G' and loss modulus G'' .

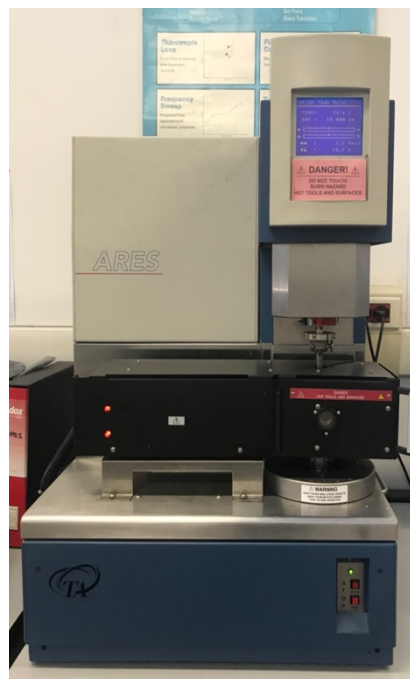


Figure 3.3 Model ARES TA Instruments rheometer.

Prior to measurement the samples were dried at 70 °C for 5h in a vacuum oven. The specimens, which are discs of about 25 mm diameter and 1 mm thickness, were prepared by compression molding with a Collin P 200 T press (Figure 3.4) with the following process parameters:

- Pressing temperature: 180 °C
- Preheating: 3 min
- degassing cycles
- Pressure: 100 bar
- Pressure holding time: 3 min

The samples were then water cooled to 50 °C and extracted from the mold.



Figure 3.4 Model P 200 T Collin press.

3.3.3 Scanning Electron Microscopy (SEM)

The morphological observations were performed using a SEM Zeiss (Oberkochen, Germany) VP Scanning Electron Microscope (beam voltage: 20kV). The cross-sections of the different samples were obtained through fracturing in liquid nitrogen and then they were coated with a gold layer before being tested. Before gold sputtering, the fractured samples were chemically treated in acetic acid for differentiation of the blend constituents, as previously done by Ravati et al. [24].

3.3.4 Mechanical measurements

Measurements of mechanical properties were performed using a Instron 5966 dynamometer (Figure 3.5) with 2kN load cell and 2kN pneumatic grips operating at 3 bar.



Figure 3.5 Model 5966 Instron dynamometer.

Tensile tests were carried out following ASTM D638-03 standard; in particular, the measurements were carried out at two different crosshead speeds: 1 mm/min until 0.5% of deformation is reached, and then 50 mm/min up to sample breakage. At least five specimens for each system were tested and the results were averaged. The specimens were prepared by injection molding with a Babyplast 6/10P Cronoplast injection machine (Figure 3.6) with different parameters for each blend to optimize the process as reported in the following tables (Table 3.4; Table 3.5). Before tensile tests the samples were kept in controlled environment at 25 °C and 30%RH for 5 days.



Figure 3.6 Model Babyplast 6/10P Cronoplast injection moulding machine.

Table 3.4 Injection molding parameters for 50PLA/30PBAT/20PHBH, 50PLA/30PBSA/10PHBH, 50PLA/30PBS/20PHBH and 50PLA/40PBS/10PHBH blends.

Parameter	50PLA/30PBAT/	50PLA/30PBSA/	50PLA/30PBS/	50PLA/40PBS/
	20PHBH	20PHBH	20PHBH	10PHBH
3 Zone temperatures (°C)	180/180/180	180/180/180	170/170/165	180/180/180
Mold temperature (°C)	18	18	18	20
Shot size (mm)	10	11	9.5	15
Cooling time (s)	10	10	10	10
1 st Injection pressure (bar)	90	90	90	100
1 st Pressure time (s)	10	10	10	20
2 nd Injection pressure (bar)	80	80	70	100
2 nd Pressure time (s)	20	20	20	20
Decompression (mm)	1	1	1	1

Table 3.5 Injection molding parameters for 40PLA/30PBS/30PHBH, 35PLA/30PBS/35PHBH, 30PLA/30PBS/40PHBH and 20PLA/30PBS/50PHBH blends.

Parameter	40PLA/30PBS/	35PLA/30PBS/	30PLA/30PBS/	20PLA/30PBS/
	30PHBH	35PHBH	40PHBH	50PHBH
3 Zone temperatures (°C)	180/180/180	170/170/170	170/170/170	170/170/170
Mold temperature (°C)	20	30	30	40
Shot size (mm)	11	19	19	19
Cooling time (s)	10	10	10	10
1 st Injection pressure (bar)	100	130	120	130
1 st Pressure time (s)	20	10	20	10
2 nd Injection pressure (bar)	90	110	100	110
2 nd Pressure time (s)	20	20	20	20
Decompression (mm)	1	1	1	1

4. Results and discussion

4.1 Selection of the most ductile blend formulation

The aim of this thesis was to enhance the elongation at break of PLA and PHBH with a much ductile polymer like PBAT, PBSA and PBS while maintaining a high modulus and a high maximum stress, characteristic of PLA and PHBH as it can be noted from Table 4.1 which reports the mechanical properties of neat polymers involved in the study. Therefore, a preliminary characterization of the tensile properties of the blends 50PLA/30PBAT/20PHBH, 50PLA/30PBSA/20PHBH and 50PLA/30PBS/20PHBH was carried out, in order to choose the most suitable formulation accomplishing the initial requirement.

Table 4.1 Main mechanical properties of pure polymers.

Property	PLA	PHBH	PBAT	PBSA	PBS
Modulus (MPa)	5144 ± 302	1568 ± 331	82 ± 7	284 ± 11	722 ± 57
Deformation at maximum stress (%)	3 ± 1	2 ± 1	28 ± 12	18 ± 2	19 ± 1
Maximum stress (MPa)	61 ± 1	24 ± 1	8 ± 1	16 ± 1	33 ± 1
Elongation at break (%)	3 ± 1	2 ± 1	623 ± 79	319 ± 15	244 ± 3
Strength at break (MPa)	61 ± 1	24 ± 1	15 ± 1	23 ± 1	39 ± 2

As it can be observed from the mechanical properties listed in Table 4.2 and from the stress-strain curve in Figure 4.1 the 50PLA/30PBAT/20PHBH blend shows a brittle behaviour, with an elongation at break of 14% which is quite low compared to 623% of pure PBAT; this result seems indicate that the introduction of PBAT does not have a beneficial effect in enhancing the ductility of this material. Furthermore, the 50PLA/30PBAT/20PHBH blend exhibited some troubles during the extrusion process, as the flow was severely unstable even after a proper adjustment in the process parameters. Therefore, due to the unsatisfactory mechanical properties, combined with poor processability, this formulation was not further explored.

Table 4.2 Mechanical properties of blend 50PLA/30PBAT/20PHBH.

Modulus (MPa)	5188 ± 1036
Deformation at maximum stress (%)	3 ± 1
Maximum stress (MPa)	40 ± 3
Elongation at break (%)	14 ± 2
Strength at break (MPa)	4 ± 1

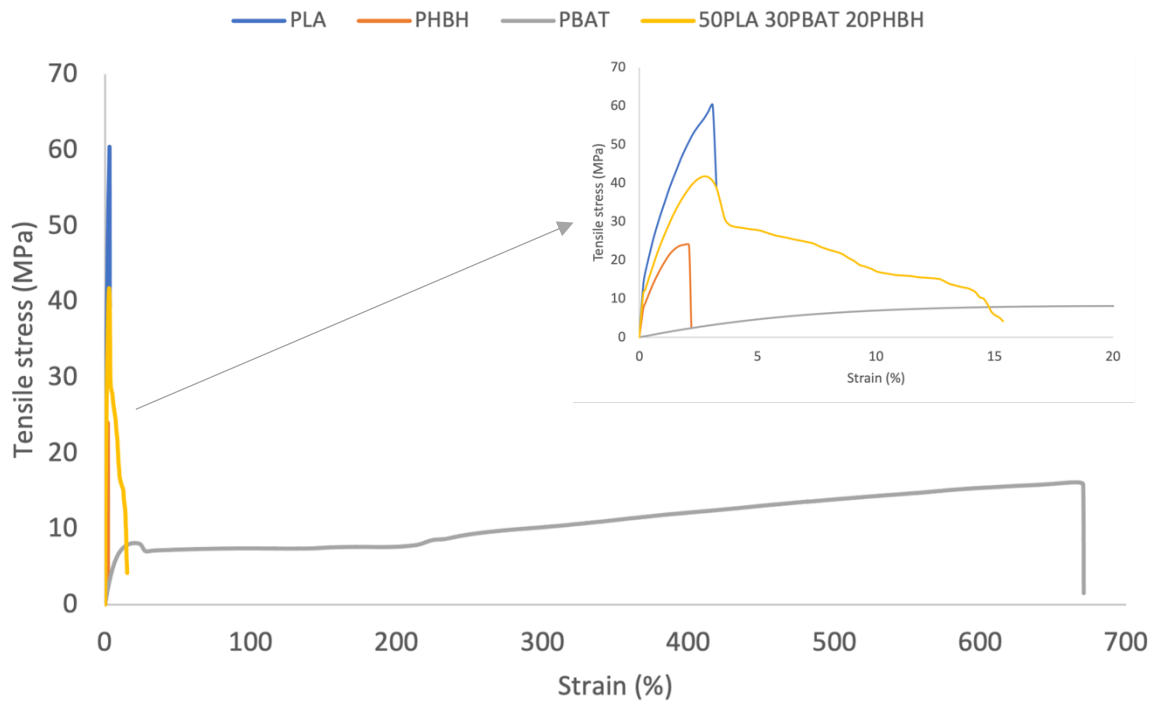


Figure 4.1 Stress-strain curve of blend 50PLA/30PBAT/20PHBH compared to PLA, PBAT and PHBH.

The 50PLA/30PBSA/20PHBH blend, as it can be observed from the mechanical properties in Table 4.3 and from the stress-strain curve in Figure 4.2, exhibits an elongation at break of 6% which is even lower than that of 50PLA/30PBAT/20PHBH blend. Also in this case, the introduction of PBSA does not provide an enhancement of the elongation at break of the blend, thus this formulation was not further explored as well.

Table 4.3 Mechanical properties of blend 50PLA/30PBSA/20PHBH.

Modulus (MPa)	2536 ± 164
Deformation at maximum stress (%)	3 ± 1
Maximum stress (MPa)	45 ± 2
Elongation at break (%)	6 ± 1
Strength at break (MPa)	21 ± 1

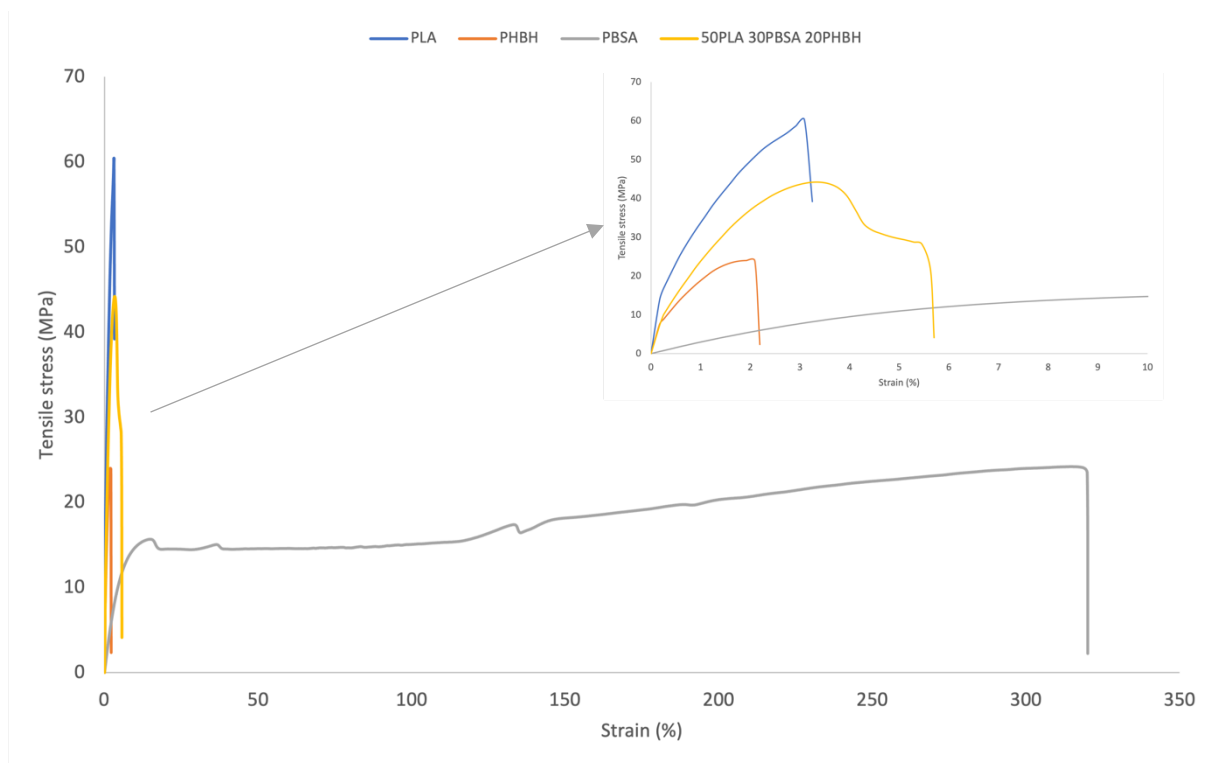


Figure 4.2 Stress-strain curve of blend 50PLA/30PBS/20PHBH compared to PLA, PBSA and PHBH.

The formulation 50PLA/30PBS/20PHBH showed consistent enhancement of mechanical properties with an increase of elongation at break up to 157% as it can be observed from Table 4.4 and Figure 4.3. Given this improvement, PBS was used for the other blend formulations, the full characterizations of which are reported in following Section 4.2.

Table 4.4 Mechanical properties of blend 50PLA/30PBS/20PHBH.

Modulus (MPa)	1841 ± 452
Deformation at maximum stress (%)	4 ± 1
Maximum stress (MPa)	43 ± 1
Elongation at break (%)	157 ± 42
Strength at break (MPa)	24 ± 4

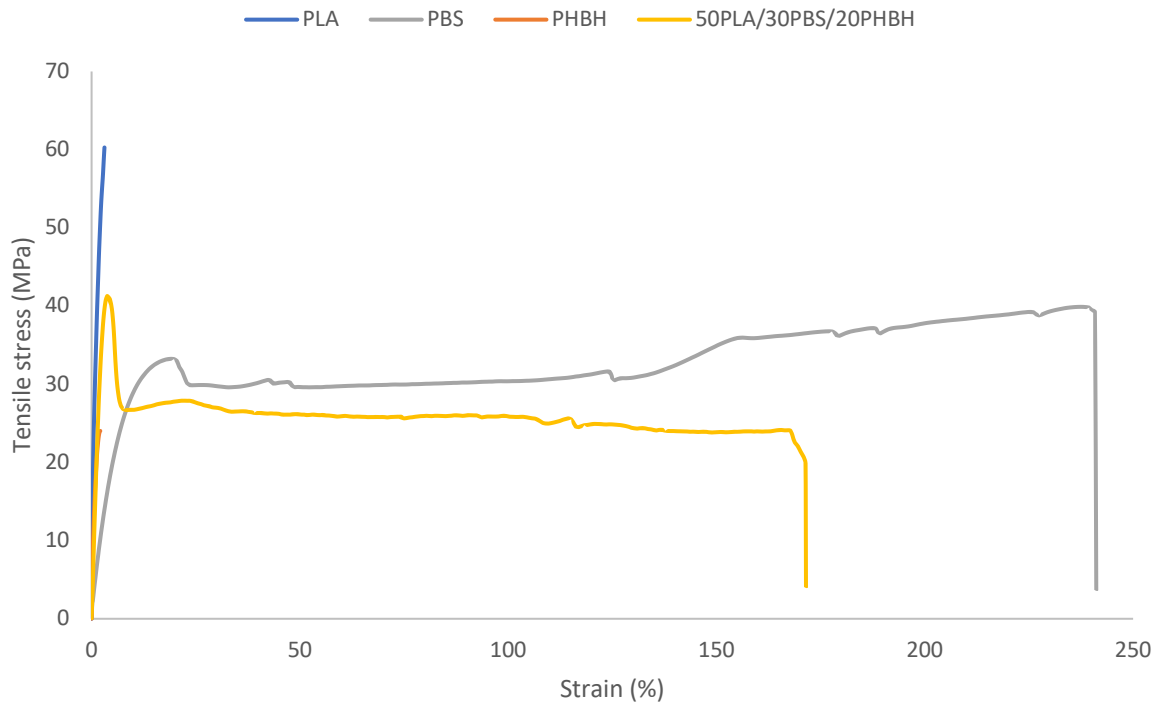


Figure 4.3 Stress-strain curve of blend 50PLA/30PBS/20PHBH compared to PLA, PBS and PHBH.

4.2 PLA/PBS/PHBH blends

The 50PLA/30PBS/20PHBH blend formulation proved to be the best at fulfilling the intended purpose, thus other formulations with varying PLA and PHBH contents were evaluated. For convenience hereinafter they will be indicated only with their composition which are summarized in the composition triangle in Figure 4.4.

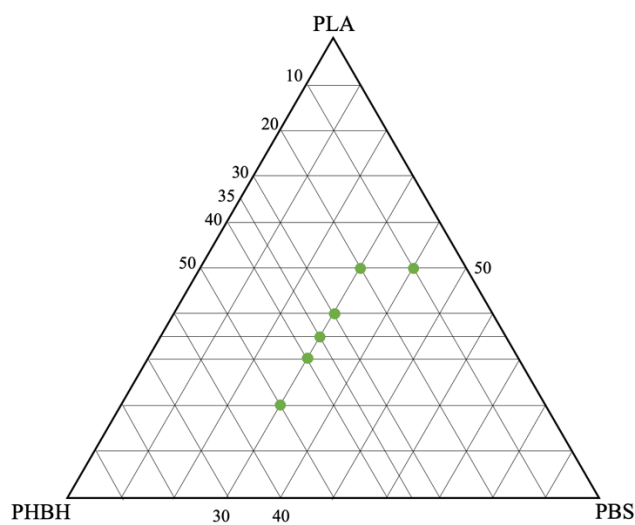


Figure 4.4 Composition triangle of PLA/PBS/PHBH blends.

4.2.1 Differential Scanning Calorimetry (DSC)

Figure 4.5 shows the cooling and second heating thermograms of neat polymers PLA, PHBH and PBS. Observing Figure 4.5a concerning neat PLA it is possible to notice:

- The absence of a crystallization peak in the cooling curve, as due to the high cooling velocity, PLA does not crystallize.
- Glass transition at 58 °C.
- An exothermic peak at 100 °C which, according to literature, can be related to cold crystallization [18].
- An endothermic peak at 169 °C corresponding to melting.

By looking at Figure 4.5b concerning neat PBS it is possible to notice:

- A crystallization peak at 85 °C.
- Glass transition at -34 °C.
- A bimodal endothermic peak at 114 °C corresponding to melting.

And finally, by observing Figure 4.5c concerning neat PHBH it is possible to notice:

- A crystallization peak at 62 °C.
- Glass transition at 3 °C.
- A bimodal endothermic peak at 148 °C corresponding to melting.

The presence of two endothermic peaks in PBS and PHBH second heating curves has been attributed to recrystallization during heating or to the thickness of the crystals [25], [26].

Table 4.5 summarizes the main thermal properties of neat polymers measured during second heating; crystallinity percentages are calculated as previously described in Section 3.3.1.

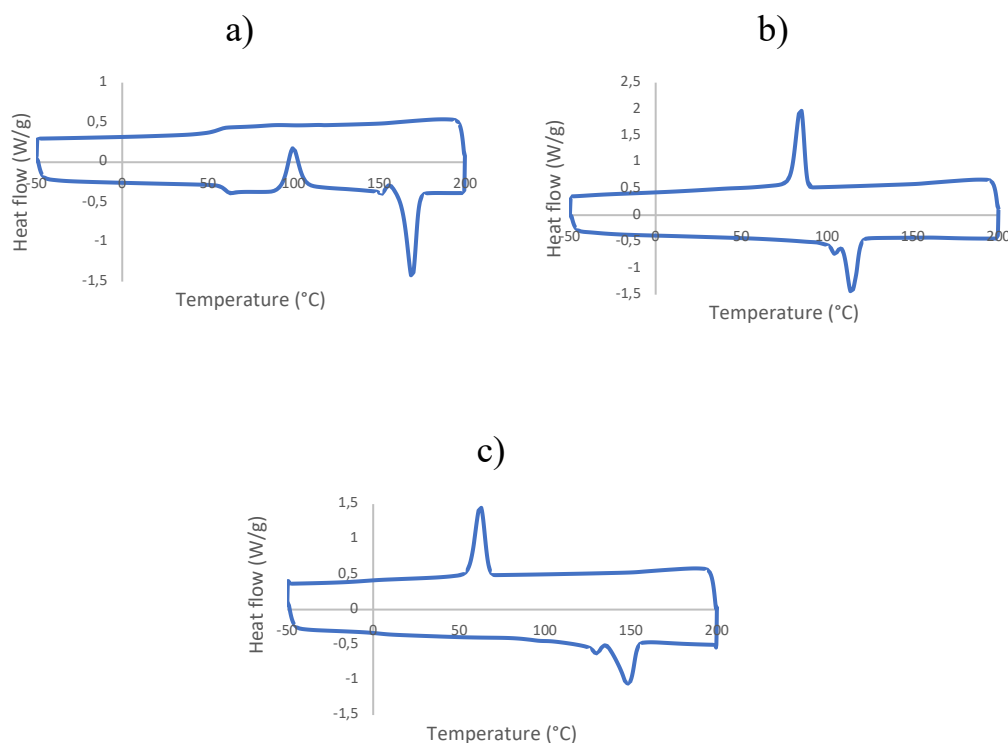


Figure 4.5 DSC cooling and second heating thermograms of neat polymers a) PLA b) PBS c) PHBH.

Table 4.5 Main thermal properties of neat polymers.

Property	PLA	PBS	PHBH
ΔH_m (J/g)	48	68	55
ΔH_{cc} (J/g)	37	-	-
χ (%)	12	60	38

Figure 4.6 shows the cooling DSC thermograms of PLA/PBS/PHBH blends compared to neat polymers. It is possible to notice how the higher the PHBH content, the more the crystallization peak of PBS shifts to low temperature until merging with crystallization peak of PHBH, thus indicating that crystallization of PBS might be restricted by the presence of PHBH, as already found by Qiu et al.[27]. On the other hand, the higher the PLA content, the more crystallization peaks of PHBH shift to lower temperature compared to neat PHBH, indicating that PLA and PBS might restrict PHBH crystallization. As previously reported in literature the decrease of crystallization rates could be caused by the dilution effect between phases which reduces the amount of chain segments toward the growing crystals [15].

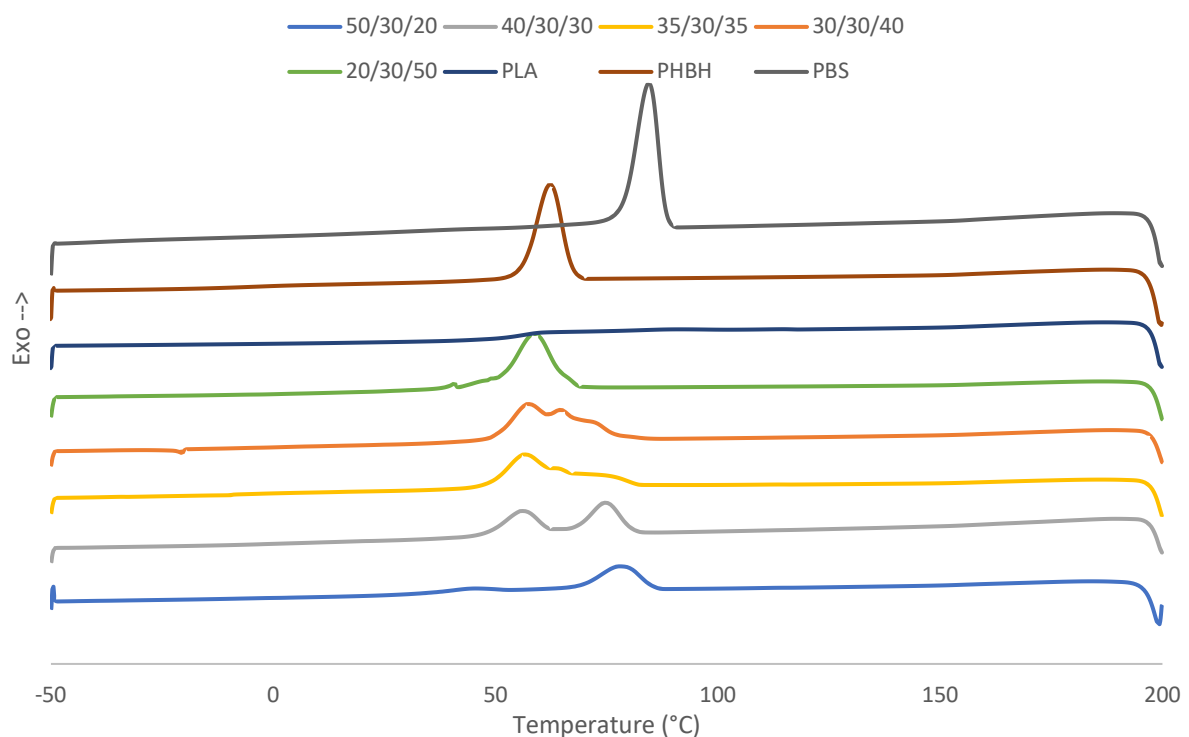
**Figure 4.6** Cooling DSC thermograms of neat polymers and PLA/PBS/PHBH blends.

Figure 4.7 shows the second heating DSC thermograms of PLA/PBS/PHBH blends compared to neat polymers. In all blends it is possible to clearly notice PLA glass transition which remains constant at around 58 °C, while for PHBH and PBS the transitions are not detectable. Also, the three endothermic peaks observed in all blends correspond to the melting of phases which for PLA, PHBH and PBS are 168 °C, 148 °C and 113 °C respectively, so they correspond to the

neat polymers melting temperatures. PLA cold crystallization temperature in the blends slightly shifts at lower temperature compared to neat PLA, this indicates that PHBH and PBS promote cold crystallization of PLA. The reason of that enhancement of cold crystallization can be attributed to the fact that, showing limited miscibility with PLA, PHBH and PBS amorphous phases could activate the chain mobility of PLA. If the locally activated chain mobility is sufficient, cold crystallization will be improved as a consequence of dynamic chain alignment. Secondly, the surface of PHBH and PBS phases might act as nucleating center thus enhancing crystallization of PLA [15].

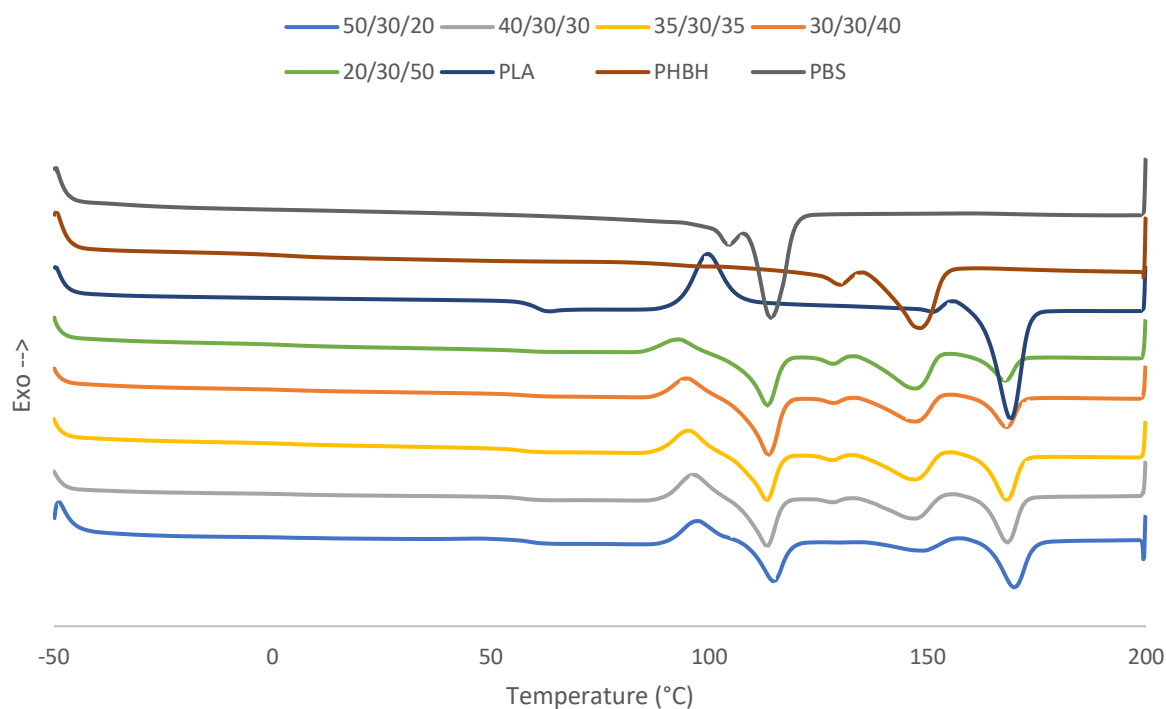


Figure 4.7 Second heating DSC thermograms of neat polymers and PLA/PBS/PHBH blends.

Table 4.6 summarizes the main thermal properties of each phase in the blends measured during second heating.

Table 4.6 Main thermal properties of PLA/PBS/PHBH blends.

Blend	Property	PLA	PBS	PHBH
50/30/20	Tg (°C)	59	-	-
	Tm (°C)	170	115	149
	ΔH_m (J/g)	21	12	7
	Tcc (°C)	97	-	-
	ΔH_{cc} (J/g)	12	-	-
	χ (%)	9	11	5
40/30/30	Tg (°C)	57	-	-
	Tm (°C)	168	113	147
	ΔH_m (J/g)	18	17	16
	Tcc (°C)	96	-	-
	ΔH_{cc} (J/g)	12	-	-
	χ (%)	6	16	11
35/30/35	Tg (°C)	57	-	-
	Tm (°C)	168	113	147
	ΔH_m (J/g)	18	17	18
	Tcc (°C)	95	-	-
	ΔH_{cc} (J/g)	13	-	-
	χ (%)	6	16	12
30/30/40	Tg (°C)	57	-	-
	Tm (°C)	168	114	148
	ΔH_m (J/g)	12	24	17
	Tcc (°C)	95	-	-
	ΔH_{cc} (J/g)	9	-	-
	χ (%)	4	22	12
20/30/50	Tg (°C)	58	-	-
	Tm (°C)	168	113	148
	ΔH_m (J/g)	10	21	22
	Tcc (°C)	93	-	-
	ΔH_{cc} (J/g)	7	-	-
	χ (%)	4	19	15

4.2.2 Rheological measurements

Complex viscosity values as a function of frequency for neat polymers are reported in Figure 4.8. PLA exhibits a Newtonian behaviour, showing a plateau for the whole investigated frequency range and a value of zero-shear viscosity of 237 Pa·s. Conversely, PBS has a remarkably non-Newtonian behaviour, as the shear-thinning region extends over the entire frequency range. Finally, PHBH exhibits a yield stress behaviour at low frequencies, which is typically observed in mineral filled polymers [28]. This behaviour is typically related to the limitation of the macromolecules relaxation caused by the restriction of chain mobility resulting from the establishment of strong filler-filler or polymer-filler interactions [29]. The presence of a mineral filler in neat PHBH was confirmed as later discussed in the following Section 4.2.3.

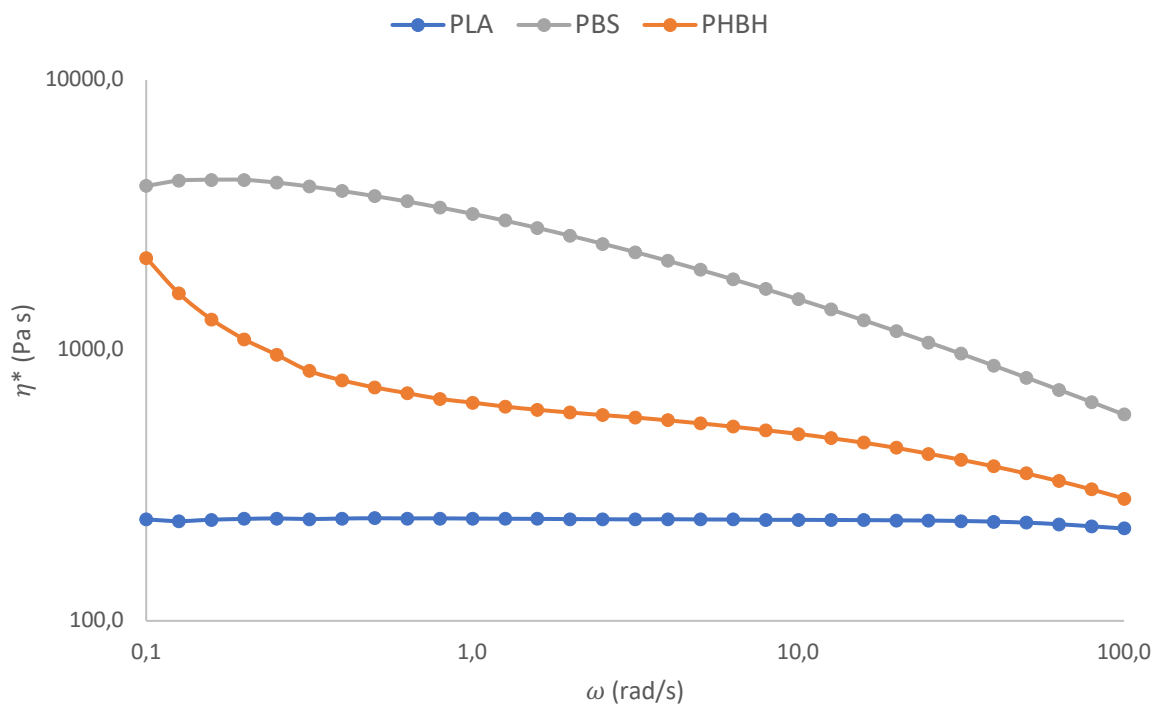


Figure 4.8 Complex viscosity curves as a function of frequency of neat polymers PLA, PBS and PHBH.

Figure 4.9 shows the complex viscosity as a function of frequency for the blends. The blends containing a higher amount of PHBH have a trend similar to neat PHBH, while the blends containing higher amount of PLA have a trend more similar to neat PLA. Generally, viscosity curves seem to be more influenced by PLA and PHBH contents, as PBS does not have a strong influence on the trend of the curves especially at higher PHBH contents; that could be related to the presence of a mineral filler in neat PHBH which strongly influence the viscosity of blends.

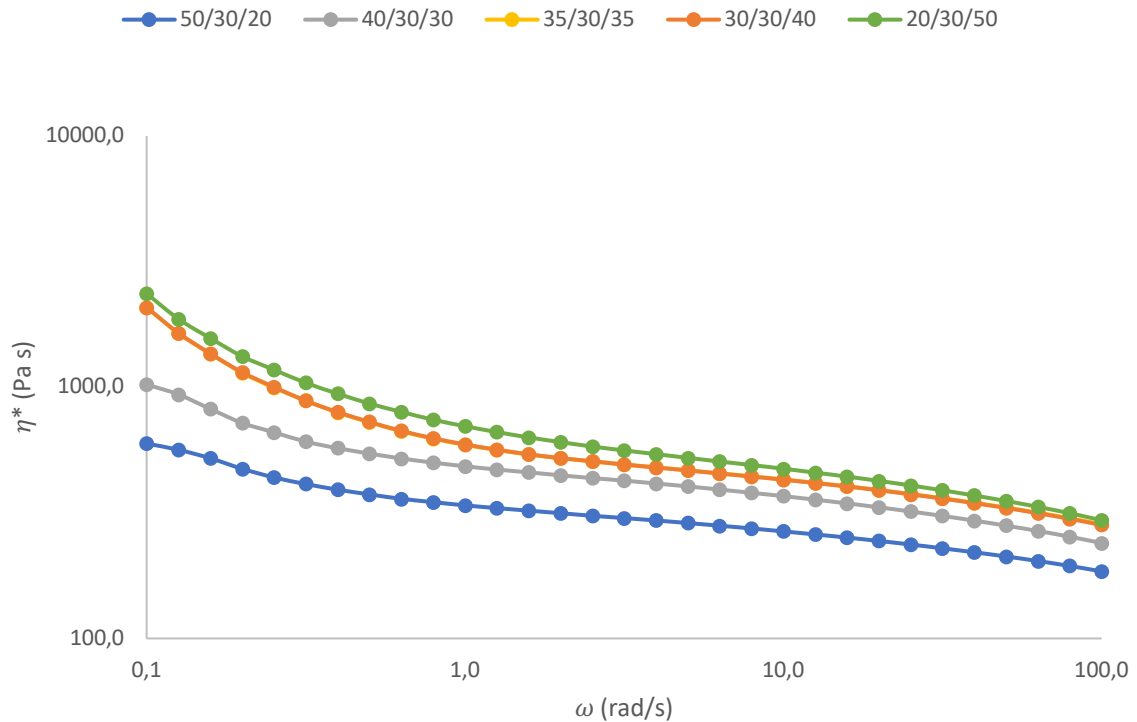


Figure 4.9 Complex viscosity curves as a function of frequency of the blends.

Figure 4.10 shows the curves related to the storage modulus G' of neat polymers, all of which exhibit the typical homopolymers behaviour. The results of the storage modulus G' measurements of the blends are reported in Figure 4.11. The curves do not exhibit the typical shoulder peak of immiscible blends, suggesting some sort of compatibility between the polymers or the achievement of a refined and homogeneous morphology. In the high frequency region, the values of G' of the blends are intermediate to those of neat polymers, indicating that the short-range dynamics of the polymer macromolecules are not affected by the presence of the interface between the phases. Differently, at low and intermediate frequencies the storage modulus of the blends shows higher values as compared to the neat polymers; this behavior is attributable an amplification of the elastic feature of the materials resulting from the triphasic morphology of the blends. In fact, the presence of interfaces between the phases and the occurrence of shape relaxation phenomenon of the dispersed phases subjected to an oscillatory shear stress, result in an increase of G' compared to neat polymers. This behaviour is more noticeable at low frequencies where the curves reflect the response of large portion of macromolecules relaxing at long times, while at higher frequencies the response of small segments able to relax faster is recorded, therefore the G' curve trend is similar to that of neat polymers [30]. Furthermore, the blends containing a higher amount of PHBH exhibit higher G' values throughout the entire frequency range, that could be associated with both the higher content of mineral filler and a more refined morphology.

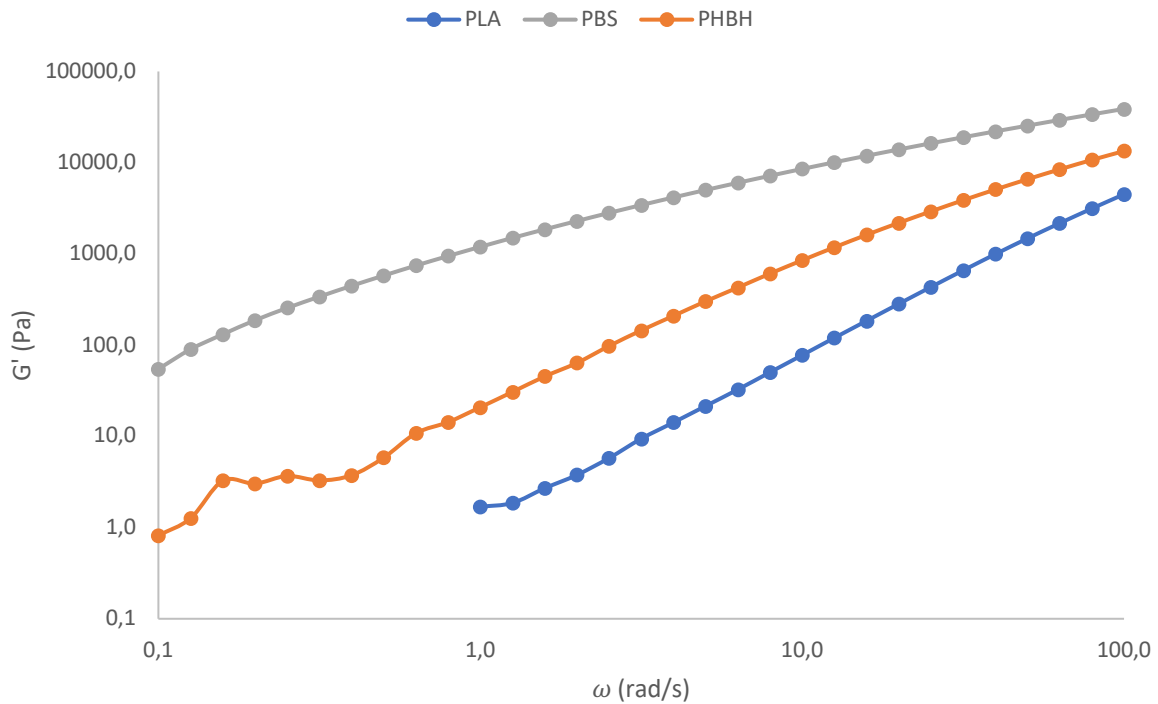


Figure 4.10 Storage modulus G' curve as a function of frequency of neat polymers PLA, PBS and PHBH.

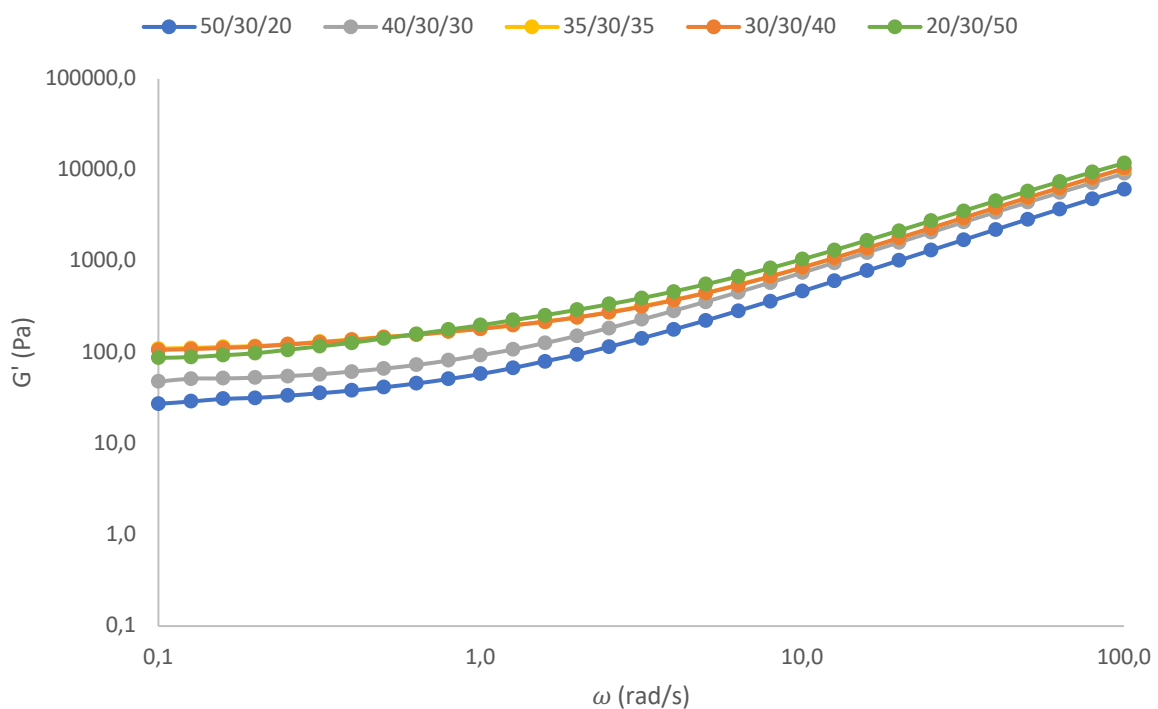


Figure 4.11 Storage modulus G' curve as a function of frequency of the blends.

The phases compatibility of the blends was studied using the criteria reported by Han Chuang which develops relationship between G' and G'' and by van Gorp which focus on the relationship between the complex modulus G^* and the phase angle δ . The two plots reported in Figure 4.12 and Figure 4.13 shows how all curves tend to merge into a common curve, which

indicates some sort of compatibility between phases that could improve their mixing and adhesion [31]. The two plots also show how the presence of talc in PHBH may be the predominant effect which conceals the effects of the dispersed phases.

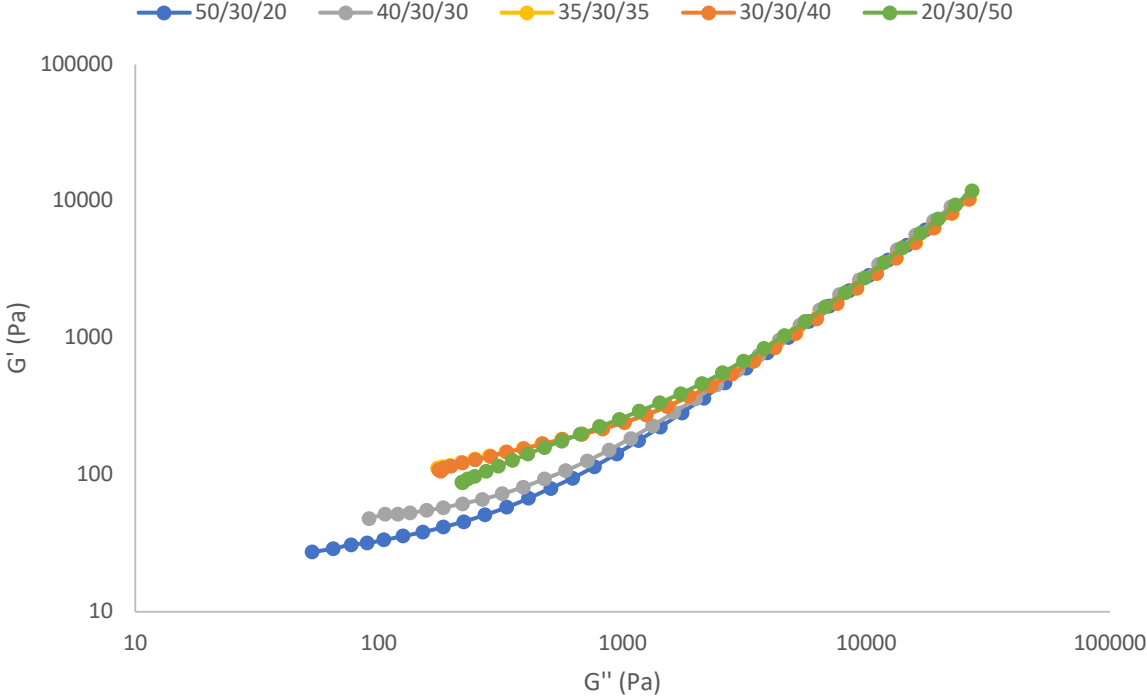


Figure 4.12 Han Chuang plot of the blends.

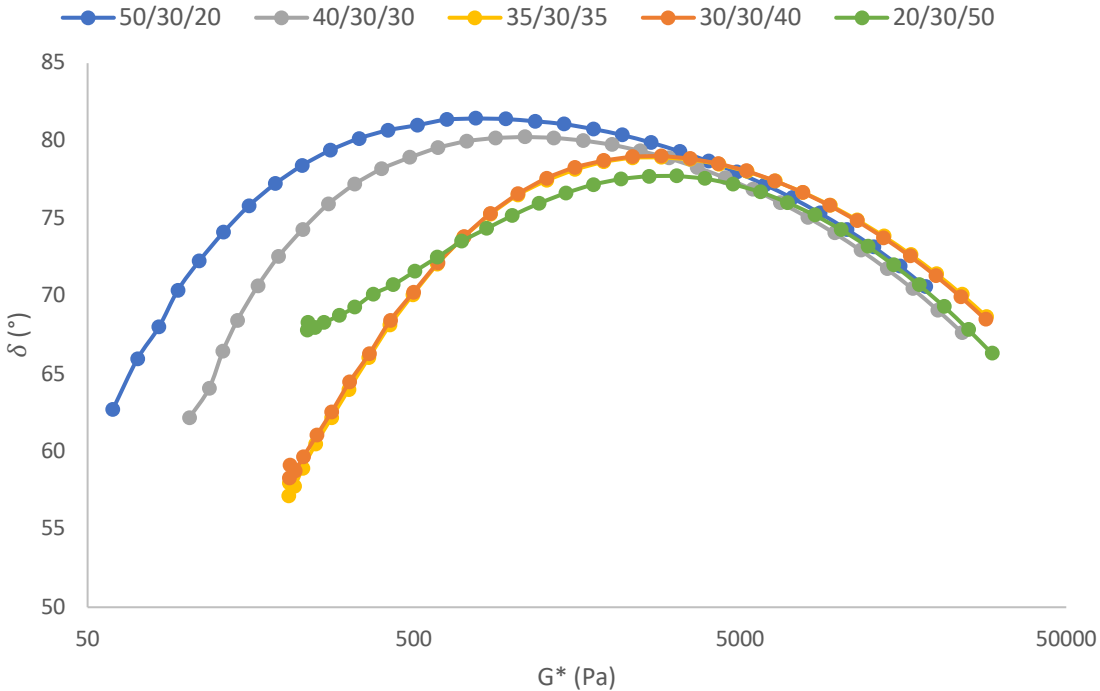


Figure 4.13 Van Gurp plot of the blends.

4.2.3 Scanning Electron Microscopy (SEM)

Figure 4.14 shows representative SEM images of 20/30/50 blend samples, either only cryo-fractured or cryo-fractured and treated in acetic acid before observation. It is possible to notice how in the treated sample (Figure 4.14a) the microstructure is much more clearly defined and, conversely, how in the untreated (Figure 4.14b) the dispersed phases are covered by a “skin” layer of material.

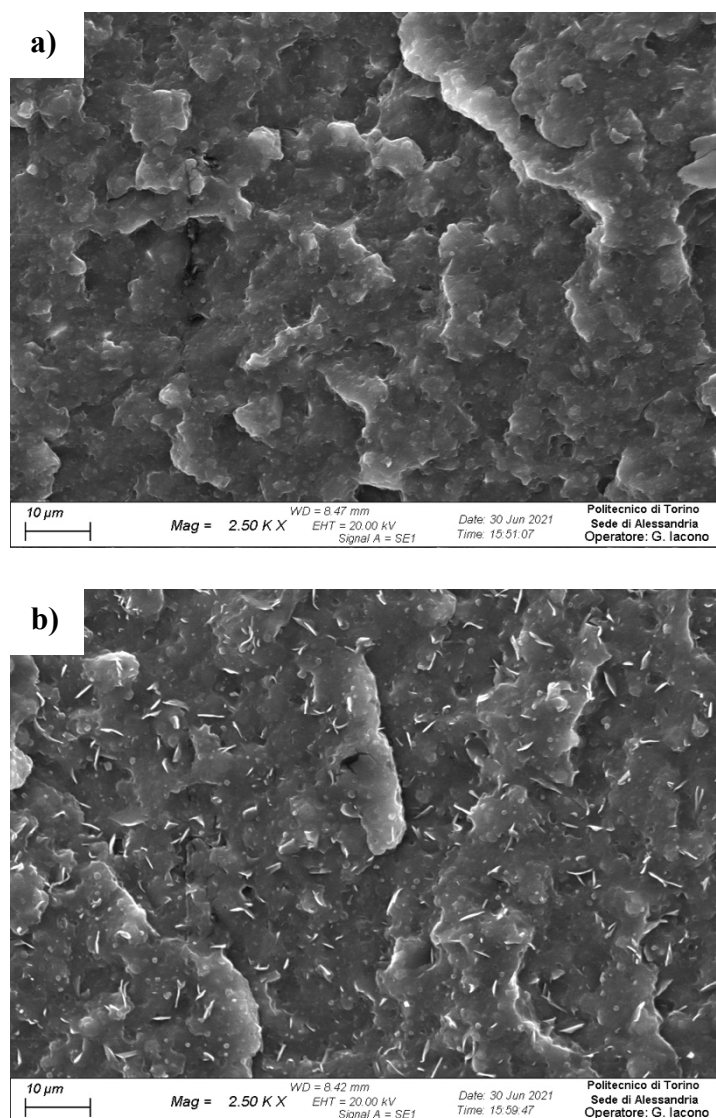


Figure 4.14 SEM images of cryo-fractured surface of 20/30/50 blend a) treated with acetic acid b) untreated.

The most noticeable feature in the untreated sample is the presence of sort of platelets, probably attributable to the presence of a mineral filler in neat PHBH as observed in Figure 4.15. To further investigate the content of a filler in PHBH, which was not declared by the supplier, the untreated sample was subjected to Energy Dispersive X-ray Spectrometry (EDS) and Thermogravimetric Analysis (TGA). The spectrum resulting from EDS analysis reported in Figure 4.16, confirmed the presence of Si and Mg, contained in talc ($Mg_3Si_4O_{10}(OH)_2$), which is normally used in biopolymers as nucleating agent [32], [33].

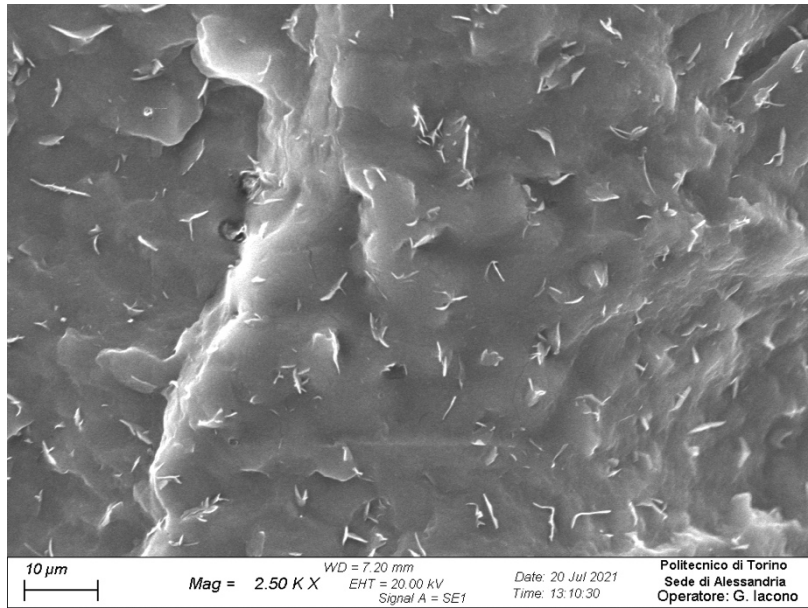


Figure 4.15 SEM image of cryo-fractured surface of neat PHBH.

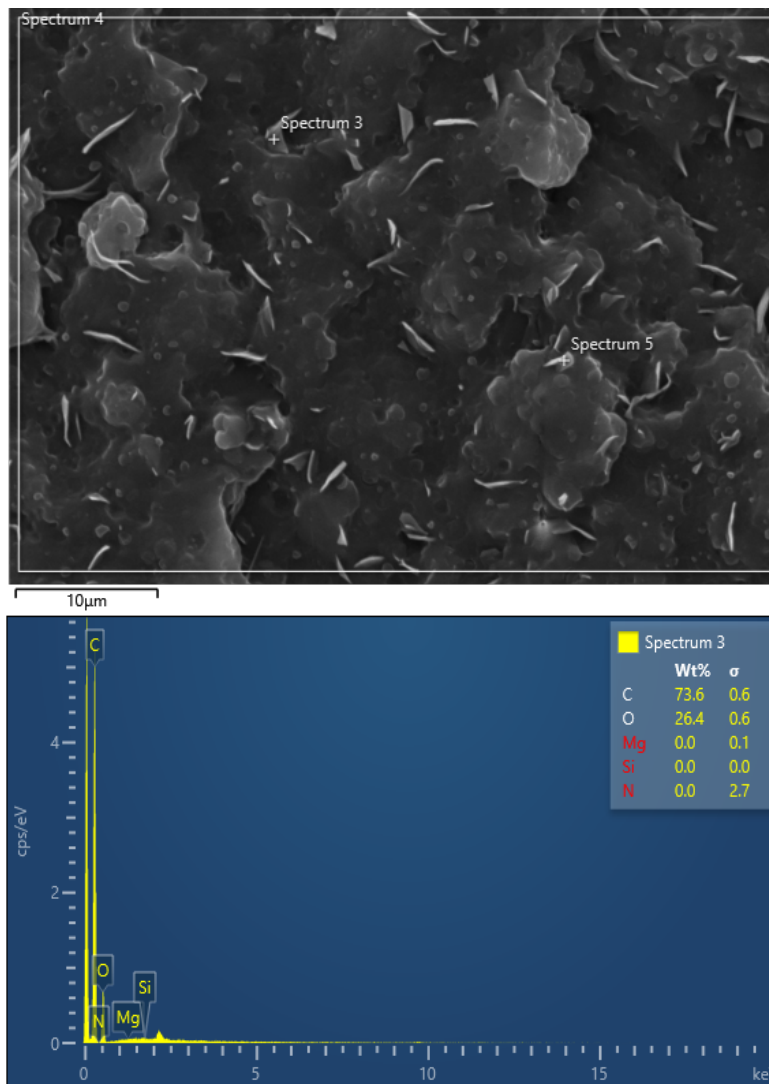


Figure 4.16 EDS spectrum of a platelet of 20/30/50 blend sample.

The curve resulting from TGA analysis reported in Figure 4.17 shows that neat PHBH has no residue at about 340 °C, that could be motivated by the low content of talc in the polymer.

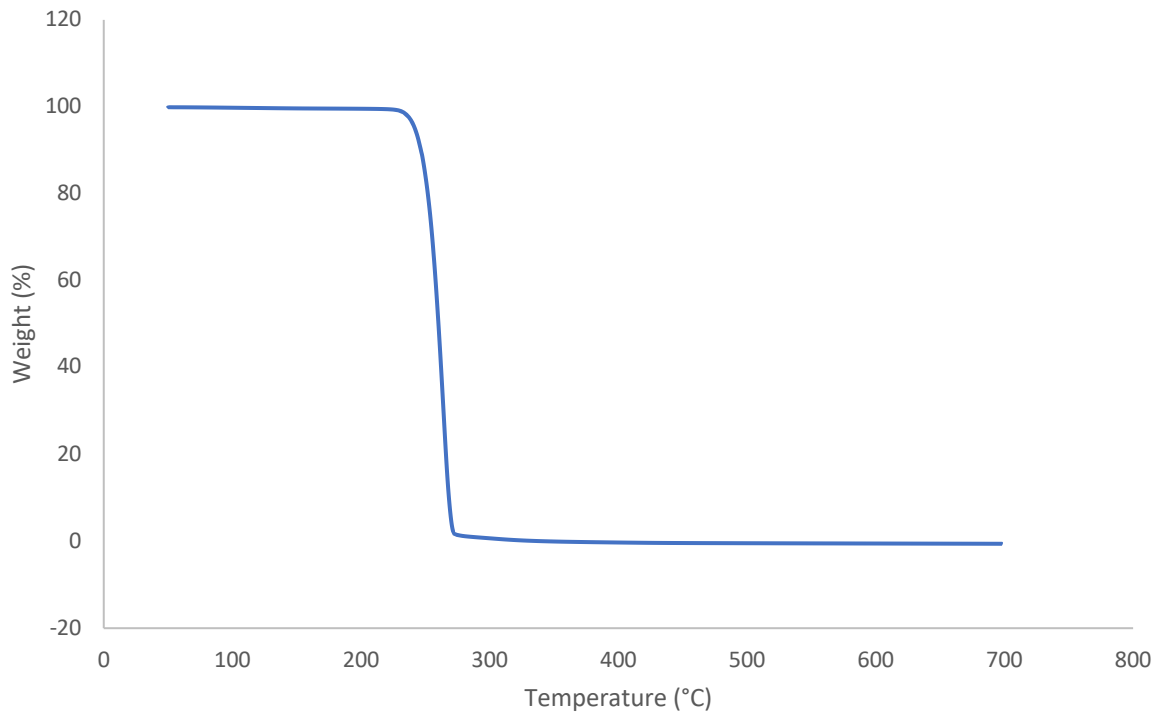


Figure 4.17 TGA analysis of neat PHBH sample.

So, the presence of small amounts of talc in PHBH has been confirmed, as well as its optimal distribution and dispersion both in neat PHBH and the blends. The yield stress behaviour observed in the rheological measurements is then attributable to the presence of the filler, which has to be considered in the further characterization of blends, especially the ones with higher content of PHBH.

Representative SEM images of the blends at 5000X magnification are reported in Figure 4.18. All the blends show a roughly droplet-like morphology with minor dispersed phases particles and dark holes left by them during fracture. The surface of the minor phases does not show clear and defined borders and seems quite rough, suggesting a certain grade of compatibility and interfacial adhesion between phases. The blends with PLA-matrix (Figure 4.18a, b) seem to have larger dispersed phases droplets. Conversely, blends with PHBH-matrix (Figure 4.18d, e) have a more refined morphology; in particular, in blend 20/30/50 the diameters of the dispersed phases are submicrometric. A finer morphology could mean higher adhesion between the phases due to the greater interfacial area, however by observing the results of the mechanical measurements in Section 4.2.4, this hypothesis will be disproved.

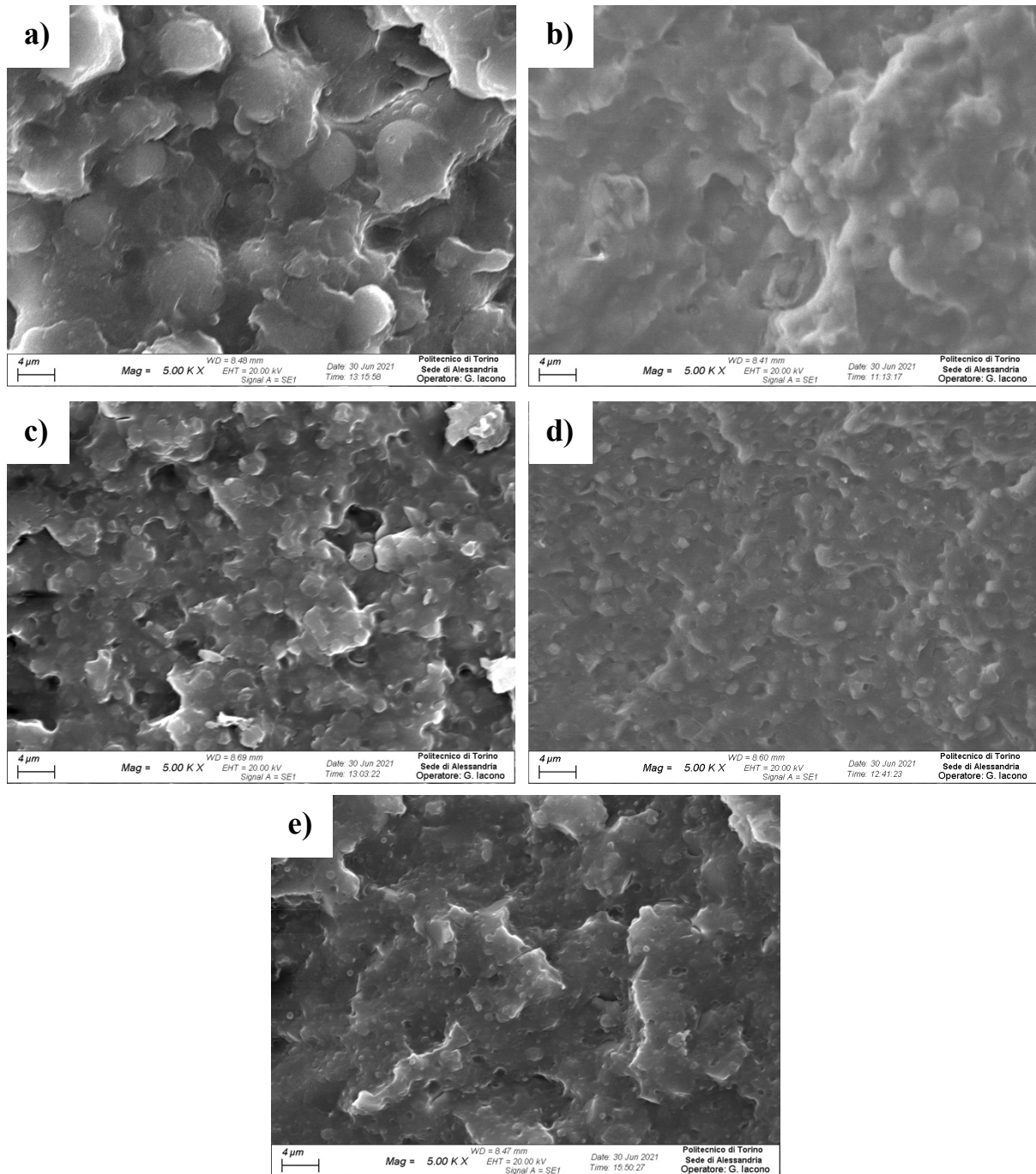


Figure 4.18 SEM images of fracture-surfaces treated with acetic acid of the blends: a) 50/30/20, b) 40/30/30, c) 35/30/35, d) 30/30/40 and e) 20/30/50 at 5000x magnification.

4.2.4 Mechanical measurements

The results of mechanical measurements on the blends are reported in Figure 4.19 and their main values are summarized in Table 4.7. Compared to neat PLA and neat PHBH which have 3% and 2% elongation respectively, all the blends show improved ductility with elongation above 7% and up to 157%. All ternary blends samples underwent yielding and their fracture behaviour was ductile, as opposed to neat PLA and neat PHBH which exhibited brittle fracture.

The maximum stress of the blends resulted to be improved compared to neat PBS and neat PHBH (33 MPa and 24 MPa respectively), ranging from 31 MPa to 43 MPa, but slightly reduced from 61 MPa of neat PLA.

The modulus ranged from 1670 MPa to 1841 MPa, which is higher compared to both neat PBS and neat PHBH, but almost 66% lower than neat PLA. The 20/30/50 blend had the lowest modulus, 1341 MPa, which is lower than neat PHBH.

As mentioned earlier, the elongation was higher than neat PLA and neat PHBH for all blends, even if just in the PLA-matrix blends the enhancement was consistent, with blend 50/30/20 and 40/30/30 having 157% and 46% elongation respectively. On the other hand, the higher the content of PHBH and the less ductile the blends are, as blend 35/30/35, 30/30/40 and 20/30/50 had just 8%, 7% and 12% elongation respectively, which is a less satisfactory result.

The toughness was calculated for each blend as mean area under the tensile stress-strain curves, the results are reported in Table 4.8. PLA-matrix blends exhibited toughness one order of magnitude higher compared to PHBH-matrix blends.

By comparing the results deriving from the DSC analysis it is possible to notice how the higher is the PHBH content and the higher are the crystallinity percentages of PHBH and PBS, while in PLA-matrix blend PHBH and PBS crystallinity percentages are rather low. A higher degree of crystallinity is in fact correlated to a more fragile behaviour, which has been confirmed by the mechanical measurements. The higher values of G' of PHBH-matrix blends deriving from the rheological measurements, which are attributable to a more refined morphology as well as the talc content, are in agreement with the more elastic, and therefore fragile, behaviour of the blends. The G' trend was attributable to the presence of interfaces between phases, as well as a refined morphology that have been confirmed by the SEM analysis. The SEM images showed a droplet-like morphology with good adhesion between phases which contributed to the good mechanical properties.

From the mechanical measurements it is possible to conclude that the combination of high stiffness and good ductility of the studied blends, which is normally impossible to be attained by neat polymers, opens applications so far inaccessible to neat PLA, PBS and PHBH alone.

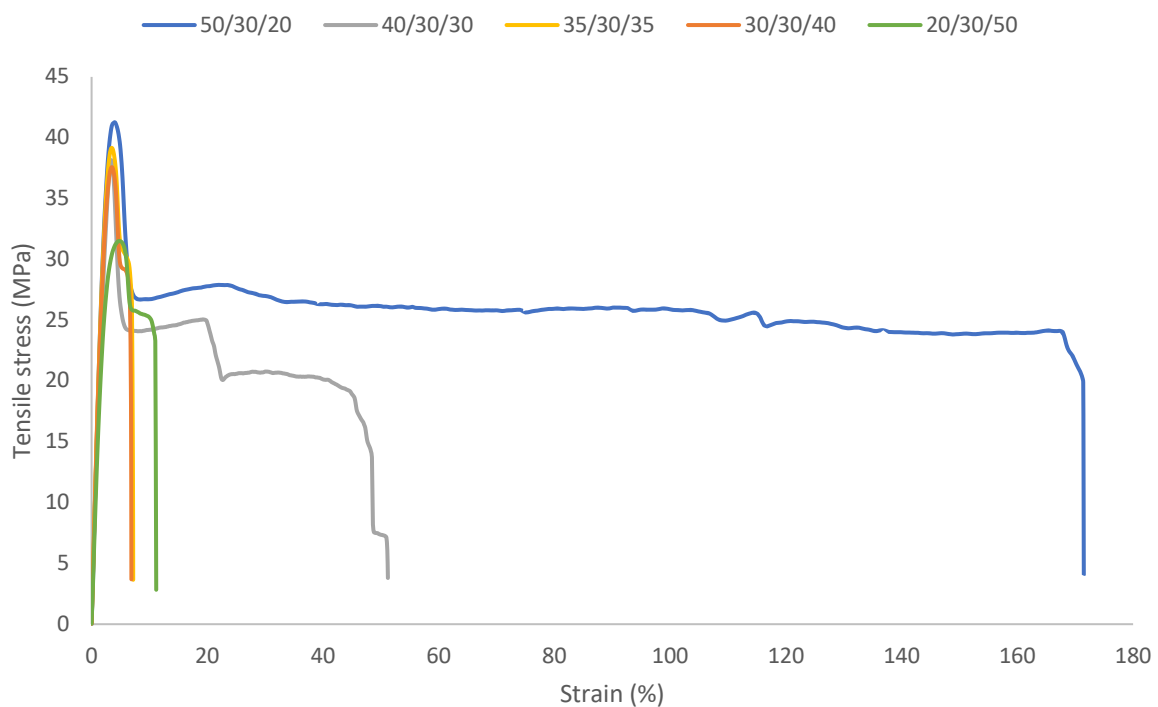


Figure 4.19 Tensile stress-strain curves of PLA/PBS/PHBH blends.

Table 4.7 Main mechanical properties of the PLA/PBS/PHBH blends.

Property	50/30/20	40/30/30	35/30/35	30/30/40	20/30/50
Modulus (MPa)	1841 ± 452	1763 ± 38	1744 ± 16	1670 ± 39	1341 ± 29
Deformation at max. stress (%)	4 ± 1	4 ± 1	3 ± 1	3 ± 1	5 ± 1
Maximum stress (MPa)	43 ± 1	42 ± 3	37 ± 3	37 ± 1	31 ± 1
Elongation at break (%)	157 ± 42	46 ± 13	8 ± 1	7 ± 1	12 ± 1
Strength at break (MPa)	24 ± 4	11 ± 9	12 ± 5	21 ± 3	19 ± 5

Table 4.8 Toughness values of the PLA/PBS/PHBH blends.

Blend	50/30/20	40/30/30	35/30/35	30/30/40	20/30/50
Toughness (J/m ³)	4124	1220	207	199	286

4.3 50PLA/40PBS/10PHBH blend

In order to further improve the elongation at break of PLA/PBS/PHBH blends, the 50/40/10 formulation was studied. The mechanical properties of the blend are reported in Table 4.9; the elongation at break was effectively enhanced at 171%, while the modulus and the maximum stress were respectively 1734 MPa and 46 MPa. So, even if the toughness was slightly lower, the 50/40/10 blend overall represented a valid alternative to 50/30/20 as a ductile material.

Table 4.9 Main mechanical properties of 50PLA/40PBS/10PHBH blend.

Modulus (MPa)	1734 ± 20
Deformation at max. stress (%)	4 ± 1
Maximum stress (MPa)	46 ± 1
Elongation at break (%)	171 ± 14
Strength at break (MPa)	5 ± 1
Toughness (J/m ³)	3417

5. Conclusions

Figure 5.1 compares the studied blends based on processability, modulus, toughness, elongation at break, availability and morphology on a scale of 0 to 3, where 3 was assigned to the blend exhibiting the best examined feature. All of the values assigned to the features derive from the results of the characterization of blends, except for processability and availability. The mechanical properties were classified by calculating the ratio, according to the proportionality principle, between the “real” values resulting from the characterization and the scale of the chart. Processability was intended as the ease of the blends extrusion process in terms of flow stability. Even though all blends were processed with the same screw profile and barrel temperature, they required different care in the adjustment of extrusion and pelletizing parameters which is reflected in the assigned values. Availability was evaluated considering the global production capacities and the weight ratio of each polymer in the blends. According to European Bioplastics the production capacity of polyhydroxyalkanoates (PHAs) is lower than that of PLA and PBS. Moreover, considering that PHBH is only a small fraction of the production of PHAs, the amount of biopolymer available per year is scarce; thus, PHBH-matrix blends are less available compared to PLA-matrix blends and have a lower value assigned in the chart [34]. Considering the price of neat polymers which is about 3 USD/kg for PLA, 5 USD/kg for PHBH and 6 USD/kg for PBS and their weight ratio, the trend of blends price can reasonably be assumed to have a similar trend as their availability [35]. However, since this parameter is more difficult to quantify compared to the other features, it has not been reported in the chart. Lastly, the best morphology was considered as the one with the smallest size domains of dispersed phases and with the most homogeneous distribution.

By observing the chart in Figure 5.1 it is possible to conclude that the 50/40/10 and 50/30/20 blends exhibit the most balanced features overall which make them suitable for applications in which high modulus and high elongation at break are both required. On the other hand, the blends containing higher amount of PHBH, 20/30/50 in particular, exhibit the finest and most homogeneous morphology, but lower mechanical properties and their use is also discouraged by reduced availability and processability.

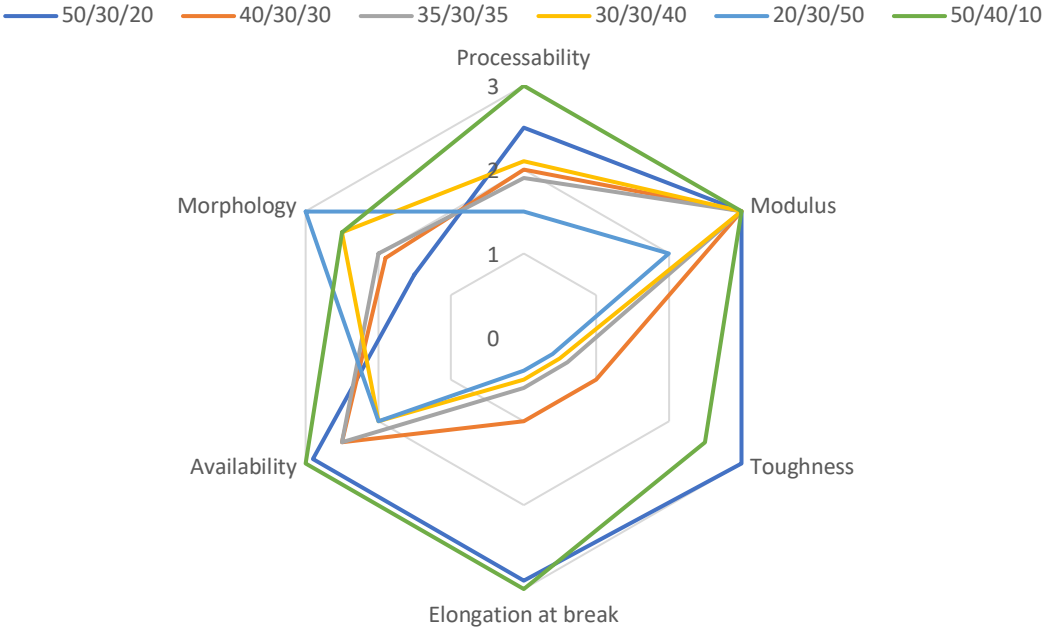


Figure 5.1 Radar chart of processability, modulus, toughness, elongation at break, availability and morphology of the blends.

6. References

- [1] S. J. Barnes, “Understanding plastics pollution: The role of economic development and technological research,” *Environ. Pollut.*, vol. 249, pp. 812–821, 2019, doi: 10.1016/j.envpol.2019.03.108.
- [2] E. Schmaltz *et al.*, “Plastic pollution solutions: emerging technologies to prevent and collect marine plastic pollution,” *Environ. Int.*, vol. 144, no. May, 2020, doi: 10.1016/j.envint.2020.106067.
- [3] K. Morrissey, “Aligning Ocean Plastic Pollution and Human Health a Co-benefits Approach,” *J. Ocean Coast. Econ.*, vol. 6, no. 1, 2019, doi: 10.15351/2373-8456.1090.
- [4] P. Li, X. Wang, M. Su, X. Zou, L. Duan, and H. Zhang, “Characteristics of Plastic Pollution in the Environment: A Review,” *Bull. Environ. Contam. Toxicol.*, no. 0123456789, 2020, doi: 10.1007/s00128-020-02820-1.
- [5] V. Goel, P. Luthra, G. S. Kapur, and S. S. V. Ramakumar, “Biodegradable/Bio-plastics: Myths and Realities,” *J. Polym. Environ.*, no. 0123456789, 2021, doi: 10.1007/s10924-021-02099-1.
- [6] Faizan Muneer, H. Nadeem, A. Arif, and W. Zaheer, “Bioplastics from Biopolymers: An Eco-Friendly and Sustainable Solution of Plastic Pollution,” *Polym. Sci. Ser. C*, vol. 63, no. 1, pp. 47–63, 2021, doi: 10.1134/s1811238221010057.
- [7] E. Kabir, R. Kaur, J. Lee, K. H. Kim, and E. E. Kwon, “Prospects of biopolymer technology as an alternative option for non-degradable plastics and sustainable management of plastic wastes,” *J. Clean. Prod.*, vol. 258, p. 120536, 2020, doi: 10.1016/j.jclepro.2020.120536.
- [8] C. J. Rhodes, “Plastic pollution and potential solutions,” *Sci. Prog.*, vol. 101, no. 3, pp. 207–260, 2018, doi: 10.3184/003685018X15294876706211.
- [9] H.-G. Elias, *Macromolecules*, vol. 4. 2011.
- [10] S. Y. Hobbs, M. E. J. Dekkers, and V. H. Watkins, “Effect of interfacial forces on polymer blend morphologies,” *Polymer (Guildf.)*, vol. 29, no. 9, pp. 1598–1602, 1988, doi: 10.1016/0032-3861(88)90269-8.
- [11] W. Witt, “Polymer Blends,” *Kunststoffe - Ger. Plast.*, vol. 74, no. 10, pp. 35–37, 1984, doi: 10.1002/0471440264.pst276.
- [12] A. Rezaei Kolahchi, A. Ajji, and P. J. Carreau, “Surface morphology and properties of ternary polymer blends: Effect of the migration of minor components,” *J. Phys. Chem. B*, vol. 118, no. 23, pp. 6316–6323, 2014, doi: 10.1021/jp502081g.

- [13] H. F. Guo, S. Packirisamy, N. V Gvozdic, and D. J. Meieri, "Prediction and manipulation morphologies of multiphase 1 . Ternary systems," *Polymer (Guildf)*., vol. 38, no. 4, pp. 785–794, 1997.
- [14] M. Nofar, D. Sacligil, P. J. Carreau, M. R. Kamal, and M. C. Heuzey, "Poly (lactic acid) blends: Processing, properties and applications," *Int. J. Biol. Macromol.*, vol. 125, pp. 307–360, 2019, doi: 10.1016/j.ijbiomac.2018.12.002.
- [15] K. Zhang, A. K. Mohanty, and M. Misra, "Fully biodegradable and biorenewable ternary blends from polylactide, poly(3-hydroxybutyrate-co-hydroxyvalerate) and poly(butylene succinate) with balanced properties," *ACS Appl. Mater. Interfaces*, vol. 4, no. 6, pp. 3091–3101, 2012, doi: 10.1021/am3004522.
- [16] M. J. Garcia-Campo, L. Quiles-Carrillo, L. Sanchez-Nacher, R. Balart, and N. Montanes, "High toughness poly(lactic acid) (PLA) formulations obtained by ternary blends with poly(3-hydroxybutyrate) (PHB) and flexible polyesters from succinic acid," *Polym. Bull.*, vol. 76, no. 4, pp. 1839–1859, 2019, doi: 10.1007/s00289-018-2475-y.
- [17] T. Yokohara and M. Yamaguchi, "Structure and properties for biomass-based polyester blends of PLA and PBS," *Eur. Polym. J.*, vol. 44, no. 3, pp. 677–685, 2008, doi: 10.1016/j.eurpolymj.2008.01.008.
- [18] A. D'Anna, R. Arrigo, and A. Frache, "PLA/PHB blends: Biocompatibilizer effects," *Polymers (Basel)*., vol. 11, no. 9, 2019, doi: 10.3390/polym11091416.
- [19] J. F. Turner, A. Riga, A. O'Connor, J. Zhang, and J. Collis, "Characterization of drawn and undrawn poly-L-lactide films by differential scanning calorimetry," *J. Therm. Anal. Calorim.*, vol. 75, no. 1, pp. 257–268, 2004, doi: 10.1023/B:JTAN.0000017347.08469.b1.
- [20] P. Xu *et al.*, "Enhanced crystallization kinetics of bacterially synthesized poly(3-hydroxybutyrate-co-3-hydroxyhexanate) with structural optimization of oxalamide compounds as nucleators," *Polym. Degrad. Stab.*, vol. 154, pp. 170–176, 2018, doi: 10.1016/j.polymdegradstab.2018.06.001.
- [21] P. A. Palsikowski, C. N. Kuchnier, I. F. Pinheiro, and A. R. Morales, "Biodegradation in Soil of PLA/PBAT Blends Compatibilized with Chain Extender," *J. Polym. Environ.*, vol. 26, no. 1, pp. 330–341, 2018, doi: 10.1007/s10924-017-0951-3.
- [22] J. A. Simão, C. F. Bellani, and M. C. Branciforti, "Thermal properties and crystallinity of PCL/PBSA/cellulose nanocrystals grafted with PCL chains," *J. Appl. Polym. Sci.*, vol. 134, no. 8, pp. 1–9, 2017, doi: 10.1002/app.44493.

- [23] E. Can, S. Bucak, E. Kinaci, A. C. Çalikoğlu, and G. T. Köse, “Polybutylene Succinate (PBS) - Polycaprolactone (PCL) Blends Compatibilized with Poly(ethylene oxide)-block-poly(propylene oxide)-block-poly(ethylene oxide) (PEO-PPO-PEO) Copolymer for Biomaterial Applications,” *Polym. - Plast. Technol. Eng.*, vol. 53, no. 11, pp. 1178–1193, 2014, doi: 10.1080/03602559.2014.886119.
- [24] S. Ravati, C. Beaulieu, A. M. Zolali, and B. D. Favis, “High performance materials based on a self-assembled multiple-percolated ternary blend,” *AIChE J.*, vol. 60, no. 8, pp. 3005–3012, Aug. 2014, doi: <https://doi.org/10.1002/aic.14495>.
- [25] B. M. P. Ferreira, C. A. C. Zavaglia, and E. A. R. Duek, “Films of PLLA/PHBV: Thermal, morphological, and mechanical characterization,” *J. Appl. Polym. Sci.*, vol. 86, no. 11, pp. 2898–2906, 2002, doi: 10.1002/app.11334.
- [26] M. E. Nichols and R. E. Robertson, “The origin of multiple melting endotherms in the thermal analysis of polymers,” *J. Polym. Sci. Part B Polym. Phys.*, vol. 30, no. 3, pp. 305–307, 1992, doi: 10.1002/polb.1992.090300311.
- [27] Z. Qiu, T. Ikehara, and T. Nishi, “Miscibility and crystallization behaviour of biodegradable blends of two aliphatic polyesters. Poly(3-hydroxybutyrate-co-hydroxyvalerate) and poly(butylene succinate) blends,” *Polymer (Guildf.)*, vol. 44, no. 24, pp. 7519–7527, 2003, doi: 10.1016/j.polymer.2003.09.029.
- [28] N. Grizzuti, *Reologia dei materiali polimerici : scienza ed ingegneria / Nino Grizzuti*. Roma: Roma : Nuova Cultura, 2012.
- [29] R. Arrigo, M. and Bartoli, and G. Malucelli, “polymers Poly (lactic Acid)– Biochar Biocomposites : E ff ect of Processing and Filler Content on Rheological ,” pp. 1–13, 2020.
- [30] F. Casamento, A. D’Anna, R. Arrigo, and A. Frache, “Rheological behavior and morphology of poly(lactic acid)/low-density polyethylene blends based on virgin and recycled polymers: Compatibilization with natural surfactants,” *J. Appl. Polym. Sci.*, vol. 138, no. 25, pp. 1–10, 2021, doi: 10.1002/app.50590.
- [31] V. Mittal, T. Akhtar, and N. Matsko, “Mechanical, thermal, rheological and morphological properties of binary and ternary blends of PLA, TPS and PCL,” *Macromol. Mater. Eng.*, vol. 300, no. 4, pp. 423–435, 2015, doi: 10.1002/mame.201400332.
- [32] W. J. Liu, H. L. Yang, Z. Wang, L. S. Dong, and J. J. Liu, “Effect of nucleating agents on the crystallization of poly(3-hydroxybutyrate-co-3-hydroxyvalerate),” *J. Appl. Polym. Sci.*, vol. 86, no. 9, pp. 2145–2152, 2002,

doi: 10.1002/app.11023.

- [33] W. Kai, Y. He, and Y. Inoue, “Fast crystallization of poly(3-hydroxybutyrate) and poly(3-hydroxybutyrate-co-3-hydroxyvalerate) with talc and boron nitride as nucleating agents,” *Polym. Int.*, vol. 54, no. 5, pp. 780–789, 2005, doi: 10.1002/pi.1758.
- [34] European Bioplastics, “Bioplastics market data.”, Jan. 2021. Accessed on: Sep. 16, 2021. [Online]. Available: <https://www.european-bioplastics.org/market/>
- [35] K. Changwichan, T. Silalertruksa, and S. H. Gheewala, “Eco-efficiency assessment of bioplastics production systems and end-of-life options,” *Sustain.*, vol. 10, no. 4, pp. 1–15, 2018, doi: 10.3390/su10040952.